Development of nucleic acid therapeutics based on the control of their intracellular distribution

2022

Keisuke Umemura

PREFACE

Humans have developed and used numerous medicines to treat diseases. It is important to deliver the required amounts of medicines to the required position for the required period of time in order to increase their effects while avoiding adverse effects. Methods to control of them have now developed as drug delivery system (DDS).[1–3] To date, clinical therapeutics based on DDS have been approved and used in clinical practice.[4,5] In recent years, antibodies, peptides, nucleic acids, and living cells have emerged in addition to conventional small molecular chemical compounds.[6] As therapeutic modalities are expanded, the necessity of DDS is also expanded to develop desirable therapeutics.[7]

In particular, nucleic acid therapeutics require drug delivery technologies.[8–10] Recently, nucleic acid therapeutics have been developed and used. In 1998, Vitravene was first approved as the nucleic acid therapeutics.[11] After that, aptamers,[12] antisense oligonucleotides,[13–16] unmethylated cytosine-phosphate-guanine (CpG) adjuvants,[17] siRNAs,[18,19] and mRNA vaccines[20] have been developed. Nucleic acids are negatively-charged water-soluble molecules, resulting in poor cellular uptake and endosomal escape. Thus, nucleic acid therapeutics are difficult to access inside of the cells. Delivery of nucleic acid therapeutics to the target site within the cells would enhance their efficacies and safety profiles. Therefore, I have focused on the strategies to control the intracellular distribution of nucleic acids.

The aim of this study is to develop functional nucleic acid therapeutics by constructing intracellular delivery strategies specific to target subcellular compartments. The laboratory I belong to, Department of Biopharmaceutics and Drug Metabolism, has reported the development of functional nucleic acids by enzymatically-constructing long single-stranded DNA (lssDNA),[21,22] and I selected lssDNA as the basis of nucleic acid therapeutics in this study. Prior to the development of intracellular targeting therapeutics, I investigated the mechanisms regarding the cellular uptake of

DNA. The density of negative charges of DNA were controlled by DNA nanotechnological methods; polypod-like DNA nanostructures (polypodna) were used. I found DNA nanostructures were mainly taken up by macrophage scavenger receptor 1 (MSR1), expressed on macrophages and dendritic cells (Chapter 1). Thus, I investigated and developed nucleic acid therapeutics that target macrophages and dendritic cells. First, to efficiently target endosomes of those cells, I attempted to develop unmethylated CpG DNA which can be sustainably retained within endosomes using i-motif DNA, responding to acidic conditions of endosomes (Chapter 2). Furthermore, I attempted to construct lssDNA which stimulates cytosolic DNA sensors by loading endosome-disruptive GALA peptides to lssDNA (Chapter 3).

In this thesis, the obtained results are discussed in three chapters below.

CONTENTS

CHAPTER 1

Critical contribution of macrophage scavenger receptor 1 to the cellular uptake of nanostructured DNA

1.1. Introduction

Endogenous and exogenous DNAs quickly disappear by nuclease digestion and cellular uptake.[8–10] Immune cells remove DNA derived from bacteria, viruses, and therapeutic DNAs.[23,24] It is important to elucidate the mechanism of DNA uptake in order to develop nucleic acid therapeutics. I selected to use DNA nanostructures to investigate the cellular uptake mechanism because DNA nanostructures with arbitrary sizes and DNA densities can be obtained by devising the nucleic acid sequences.

DNA can self-assemble through Watson-Crick base pairing.[25] These characteristics can be used to create nanometer-sized DNA structures with arbitrary shapes.[26,27] This approach, which is called DNA nanotechnology, has been progressing rapidly in recent years. It was pioneered by Seeman *et al*., who created DNA junctions and DNA lattices.[28] Rothemund *et al*. developed a DNA origami technology, in which a long single-stranded "scaffold" DNA and short "staple" DNAs are annealed into a programmed shape by self-assembly.[29] Furthermore, various nanostructured DNAs have been developed.[30,31]

Previous results from our group showed that polypod-like nanostructured DNA, or polypodna, consisting of three or more oligodeoxynucleotides (ODNs), were efficiently taken up by various murine and human immune cells such as macrophages and dendritic cells.[32–34] Cellular uptake of polypodna has reported to be pod number-dependently. When unmethylated cytosine-phosphate-guanine (CpG) DNA, which is a ligand of Toll-like receptor 9 (TLR9), was incorporated into polypodna, the CpG DNA-mediated release of immunostimulatory cytokines from immune cells was significantly increased.

Polypodna is taken up by immune cells more efficiently as the pod number increases.[32–34] Since the increase in pod number results in the increase of negative charge density, our group has investigated and reported the relationships between the density of negative charges of DNA and the

cellular uptake.[35] DNA origami technology was used to vary the densities of negative charges, and it was revealed that DNA nanostructures with high negative charge density resulted in the increase in cellular uptake by immune cells.

Elucidating the mechanisms of the cellular uptake of DNA and the receptors or membrane proteins involved in the uptake would lead to the theoretical design of efficient delivery systems of CpG DNA and other nucleic acid therapeutics. Despite the importance of the cellular uptake of DNA, its detailed mechanism has not been elucidated. Concerning the cellular uptake of single- or double-stranded, phosphodiester (PO) or chemically-modified phosphorothioate (PS) ODNs, various kinds of receptors/membrane proteins have been reported to be involved, including macrophage scavenger receptor 1 (MSR1, SR-A1),[36] macrophage-1 antigen (MAC-1),[37] advanced glycosylation end product-specific receptor (AGER),[38] membrane-associated nucleic acid-binding protein (MNAB),[39] DEC-205,[40] and macrophage mannose receptor 1 (MRC1).[41] However, in most cases, their involvement in DNA uptake has been examined using PS DNA, which non-specifically binds to both soluble and membrane proteins.[42,43] Therefore, the results obtained using PS DNA might not be applied to natural, phosphodiester (PO) DNA, which has different binding characteristics from PS DNA. Among these receptors and membrane proteins, MSR1 has been reported to be involved in the uptake of PO DNA by macrophages.[42] Based on these considerations, our group has focused on MSR1 as a receptor for the uptake of PO DNA and revealed that MSR1 was involved in the cellular uptake of PO single-stranded DNA (ssDNA) and tetrapod-like nanostructured DNA (tetrapodna) by using HEK-Blue hTLR9 cells transfected with *MSR1*.[44]

Despite these findings, however, little is known about the receptors that are responsible for the cell type-specific and pod number-dependent uptake of polypodna. The following questions still remain unveiled and need to be answered: (1) what are the receptors responsible for the efficient uptake of DNA nanostructures; (2) how much MSR1 contributes to the uptake; and (3) the reason why the

uptake of DNA nanostructures by immune cells is more efficient than that of single-stranded ODNs by immune cells. Answering these questions will help develop targeted delivery systems of DNA therapeutics.

The objective of CHAPTER 1 is, therefore, to elucidate the contribution of MSR1 and other receptors to the cellular uptake of polypodna. Herein, I show that MSR1 plays a dominant role in the pod number-dependent uptake of DNA in MSR1-expressing immune cells, including macrophages and dendritic cells.

1.2. Materials & Methods

1.2.1. Chemicals

Dulbecco's modified Eagle medium (DMEM) and Roswell Park Memorial Institute (RPMI) 1640 medium were obtained from Nissui Pharmaceutical Co., Ltd. (Tokyo, Japan). Opti-MEM and fetal bovine serum (FBS) were purchased from Thermo Fisher Scientific Inc. (Waltham, MA). Blasticidin, zeocin, and normocin were obtained from InvivoGen (San Diego, CA). Lipopolysaccharides from Escherichia coli O55:B5 were purchased from Sigma-Aldrich Co. LLC (St. Louis, MO). Sodium chloride, sodium hydrogen phosphate, sodium bicarbonate, potassium chloride, glucose, and sodium dodecyl sulfate (SDS) were obtained from FUJIFILM Wako Pure Chemical Corporation (Osaka, Japan). All other chemicals were of the highest grade available and were used without further purification.

1.2.2. ODNs and preparation of polypodna

PO ODNs and PS-modified CpG ODN 1668 were obtained from Integrated DNA Technologies, Inc. (Coralville, IA). The sequences of the ODNs studied are shown in Table 1. ODN-1, an 18-base long PO DNA, was used as an ssDNA and a component of polypodnas. Polypodnas were prepared as follows: equimolar amounts of ODNs were mixed, i.e., hexa1-6 and a six-fold molar excess of ODN-1 for hexapodna; hexa1-4, penta5, and a five-fold molar excess of ODN-1 for pentapodna; hexa1-3, tetra4, and a four-molar excess of ODN-1 for tetrapodna; hexa1, 2, tri3, and a three-molar excess of ODN-1 for tripodna; and ODN-1 and dsDNA2 for dsDNA. The mixed ODNs were annealed in sterile water containing 150 mM sodium chloride in a thermal cycler. The formation was confirmed by polyacrylamide gel electrophoresis (PAGE, 6%, 37.5:1 acrylamide/bisacrylamide). The gel was run at 22-25 °C at 200 V for 20 min in 1 × TBE buffer.

Table 1. Sequences of the ODNs.

Name	Sequences (5′ → 3′)	Length (bases)
ODN-1	GAGACGTTCTCACCGAAT	18
Hexa1	GCTTGAATCCATGAGCTG GGTTGTATGACTGCAAGC ATTCGGTGAGAACGTCTC	54
Hexa2	GCTTGCAGTCATACAACC AATCCTGAGCCTCTGAGC ATTCGGTGAGAACGTCTC	54
Hexa3	GCTCAGAGGCTCAGGATT CCGCTTCATCAGTATAGC ATTCGGTGAGAACGTCTC	54
Hexa4	GCTATACTGATGAAGCGG TGAAGTGAGCTCTCAAGC ATTCGGTGAGAACGTCTC	54
Hexa5	GCTTGAGAGCTCACTTCA ATATGCAGCTCTGAGAGC ATTCGGTGAGAACGTCTC	54
Hexa6	GCTCTCAGAGCTGCATAT CAGCTCATGGATTCAAGC ATTCGGTGAGAACGTCTC	54
dsDNA2	ATTCGGTGAGAACGTCTC	18
Tri3	GCTCAGAGGCTCAGGATT CAGCTCATGGATTCAAGC ATTCGGTGAGAACGTCTC	54
Tetra4	GCTATACTGATGAAGCGG CAGCTCATGGATTCAAGC ATTCGGTGAGAACGTCTC	54
Penta5	GCTTGAGAGCTCACTTCA CAGCTCATGGATTCAAGC ATTCGGTGAGAACGTCTC	54
ODN1668	T*C*C*A*T*G*A*C*G*T*T*C*C*T*G*A*T*G*C*T	20

The sequence of the CpG motif is underlined. PS linkages are notated by asterisks.

1.2.3. Cells

HEK-Blue hTLR9 cells were obtained from InvivoGen and cultured in DMEM supplemented with 10% heat-inactivated FBS, 0.2% sodium bicarbonate, 100 IU/mL penicillin, 100 μg/mL streptomycin, 2 mM L-glutamine, 30 μg/mL blasticidin, 100 μg/mL zeocin, and 100 μg/mL normocin. Murine macrophage-like RAW264.7 cells were purchased from ATCC (Manassas, VA) and cultured in RPMI1640 medium supplemented with 10% heat-inactivated FBS, 0.2% sodium

bicarbonate, 100 IU/mL penicillin, 100 μg/mL streptomycin, and 2 mM L-glutamine. All cells were cultured at 37 °C in humidified air containing 5% CO_2.

Peritoneal macrophages and bone marrow-derived dendritic cells (BMDCs) were obtained from six-week-old female BALB/c mice, which were purchased from Japan SLC, Inc. (Hamamatsu, Japan). To obtain peritoneal macrophages, mice were peritoneally injected with TGC medium (Nissui Pharmaceutical Co., Ltd.) 4 days previously. BMDCs were differentiated from bone marrow cells of femurs and tibias. Bone marrow cells were cultured with 20 ng/mL recombinant GM-CSF (PeproTech Inc., Rocky Hill, NJ) for 6 days and the culture medium was changed every 2 days. Finally, non-adherent cells were harvested and used as BMDCs. Protocols for the experiments using mice were approved by the Animal Experimentation Committee of the Graduate School of Pharmaceutical Sciences, Kyoto University.

1.2.4. Transfection

A plasmid vector encoding human *MSR1* was constructed by insertion of FLAG-tagged *MSR1* cDNA into the multi-cloning site of pcDNA3.1(+) (Thermo Fisher Scientific Inc.). HEK-Blue hTLR9 cells were transfected with the plasmid using Lipofectamine 2000 (Thermo Fisher Scientific Inc.) according to the manufacturer's protocol.

1.2.5. Gene knockout

Murine *Msr1*-targeted CRISPR RNA (crRNA), trans-activating CRISPR RNA (tracrRNA), and Cas9 nuclease were obtained from Integrated DNA Technologies, Inc. crRNA sequences were prepared for three sites of the murine *Msr1* gene,[45] and the targeted sequences are shown in Table 2. RAW264.7 cells were seeded in a 24-well plate at a density of 2.5×10^5 cells/well, and were transfected with a complex of crRNA, tracrRNA, and Cas9 using Lipofectamine RNAiMAX (Thermo Fisher

Scientific Inc.). The transfected cells were incubated for 48 h and replated in a 96-well plate at a density of 1 cell/well, and *Msr1*-knockout cell clones were established. To confirm *Msr1*-knockout, a cell lysate of each clone was analyzed by western blotting using an anti-mSR-A1/MSR1 antibody (AF1797; R&D Systems, Inc., Minneapolis, MN).

Table 2. The targeted sequences of the *Msr1* gene for the knockout.

	Position	Sequences (5′ → 3′)
1	Chromosome 8 39619982 – 39620002	AGAACAAGCGCACGTGGAAC
2	Chromosome 8 39631294 – 39631314	GCAGTACTAATACCTGTTGT
3	Chromosome 8 39624143 – 39624163	AAAAGCCGACCTTATAGACA

1.2.6. Cellular uptake of polypodna

ODN-1 labeled with Alexa Fluor 488 at the 5′ end was obtained from Japan Bio Services Co., Ltd. (Saitama, Japan). Dextran sulfate sodium (Nacalai Tesque, Kyoto, Japan) was used as a scavenger receptor inhibitor at a concentration of 5 mg/mL. HEK-Blue hTLR9 cells or RAW264.7 cells were seeded on 48- or 96-well plates at a density of 1×10^5 cells/well or 5×10^4 cells/well, respectively, and cultured for 24 h. The cells were then incubated with 0.5 μM Alexa Fluor 488-labeled ODN-1 (ssDNA) and polypodnas loaded with Alexa Fluor 488-labeled ODN-1 for 2 h at 37 °C. The concentration of Alexa Fluor 488-labeled DNA in each sample was adjusted to contain 0.5 μM Alexa Fluor 488-labeled ODN-1. The fluorescence intensity of all the Alexa Fluor 488-labeled DNA samples were confirmed to be comparable prior to addition to cells. The cells were washed three times with phosphate-buffered saline (PBS) and harvested. The fluorescence intensity of the cells was determined by flow cytometry (Gallios Flow Cytometer; Beckman Coulter, Inc., Brea, CA) and the mean

fluorescence intensity (MFI) of 1×10^4 cells were calculated using Kaluza software (version 1.0; BD Biosciences, San Jose, CA).

1.2.7. TNF-α release from RAW264.7 cells

Wild-type and *Msr1*-knockout RAW264.7 cells were seeded on 96-well plates at a density of 5×10^4 cells/well and cultured for 24 h. The cells were then incubated with 0.5 μM ODN-1 and ODN-1-loaded polypodnas (the concentration of ODN-1 was 0.5 μM), 0.25μM PS ODN 1668 and 5 ng/mL lipopolysaccharide for 8 h at 37 °C. The levels of TNF-α in the supernatants were determined by enzyme-linked immunosorbent assay (ELISA) using a Mouse TNF (Mono/Mono) ELISA Set (BD Biosciences).

1.2.8. Western blotting

A fraction of cell lysates or protein solutions were reduced by 100 mM dithiothreitol, subjected to 10% SDS-PAGE, and transferred to a polyvinylidene fluoride transfer membrane (Immobilon-P; Merck Millipore, Burlington, MA). The membrane was blocked by Blocking One (Nacalai Tesque) and incubated with anti-mSR-A1/MSR1 polyclonal antibody (AF1797) or anti-GAPDH monoclonal antibody (ab8245; Abcam plc., Cambridge, UK) for 1 h at room temperature (22-25 °C). The membrane was then incubated with horseradish peroxidase (HRP)-conjugated donkey anti-goat IgG antibody (Santa Cruz Biotechnology, Inc., Dallas, TX) or HRP-conjugated goat anti-mouse IgG antibody (Bethyl Laboratories, Inc., Montgomery, TX), respectively, for 1 h at room temperature. Protein bands were detected by chemiluminescence using an Immobilon Western Chemiluminescent HRP substrate (Merck Millipore).

1.2.9. DNA-receptor crosslinking and pull-down of receptors

Biotinylated ODN-1 at the 5′ end was obtained from Japan Bio Services Co., Ltd. Cells were seeded on a 15-cm dish at a density of 1×10^7 cells/well and cultured for 24 h. The cells were incubated on ice for 30 min and then incubated with 0.5 μM biotinylated ODN-1 in the form of either ssDNA, tetrapodna, or hexapodna for 30 min on ice. Biotinylated DNA and its cell surface receptors, if any, were crosslinked with 4% paraformaldehyde (PFA) for 30 min at room temperature. The cells were washed three times with PBS, and lysed with RIPA buffer (50 mM Tris-HCl; pH 7.6, 150 mM NaCl, 0.5 w/v% sodium deoxycholate, 0.1 w/v% SDS, 0.1 v/v% Triton X-100, and 1 v/v% Nonidet P-40) containing a protease inhibitor cocktail (Nacalai Tesque). Clear lysate was obtained by centrifugation at 16,000 *g* for 20 min. Streptavidin magnetic beads (New England BioLabs, Ipswich, MA) were blocked with 1% bovine serum albumin (Reagent Diluent Concentrate 2; R&D Systems, Inc.) for 1 h and incubated with the lysate for 1 h. The beads were collected using a magnet and washed five times with RIPA buffer. Proteins pulled-down by the beads were eluted by boiling at 95 °C for 5 min in SDS-PAGE sample buffer (78 mM Tris-HCl; pH 6.8, 6.3 w/v% sucrose, and 2.5 w/v% SDS).

1.2.10. Statistical analysis

Differences were statistically evaluated by Student's t-tests for comparisons between two groups. *P* values less than 0.05 were considered statistically significant.

1.3. Results

1.3.1. ODN-1-loaded polypodnas were formed.

Figure 1A shows the schematic illustration of ODN-1-loaded hexapodna. Figure 1B shows the PAGE analysis of polypodna used in this study. Each lane had a major single band with migration depending on the number of bases per polypodna. To evaluate the cellular uptake of polypodna or its binding to MSR1, we prepared fluorescently labeled or biotinylated polypodna. ODN-1 was labeled with Alexa Fluor 488 or biotin at the 5′ end and ODN-1 was annealed with other ODNs consisting of polypodna. Formation of Alexa Fluor 488-lebeled or biotinylated polypodna used in this study was also confirmed by PAGE analysis (Figure 2). These results indicated the successful formation of polypodnas with or without Alexa Fluor 488-labeling or biotinylation of ODN-1. In addition, to confirm whether polypodnas are intact after incubation with cells, polypodnas incubated with RAW264.7 cells were analyzed by PAGE. Almost no significant changes in the bands of polypodnas were observed in the PAGE analysis (Figure 3).

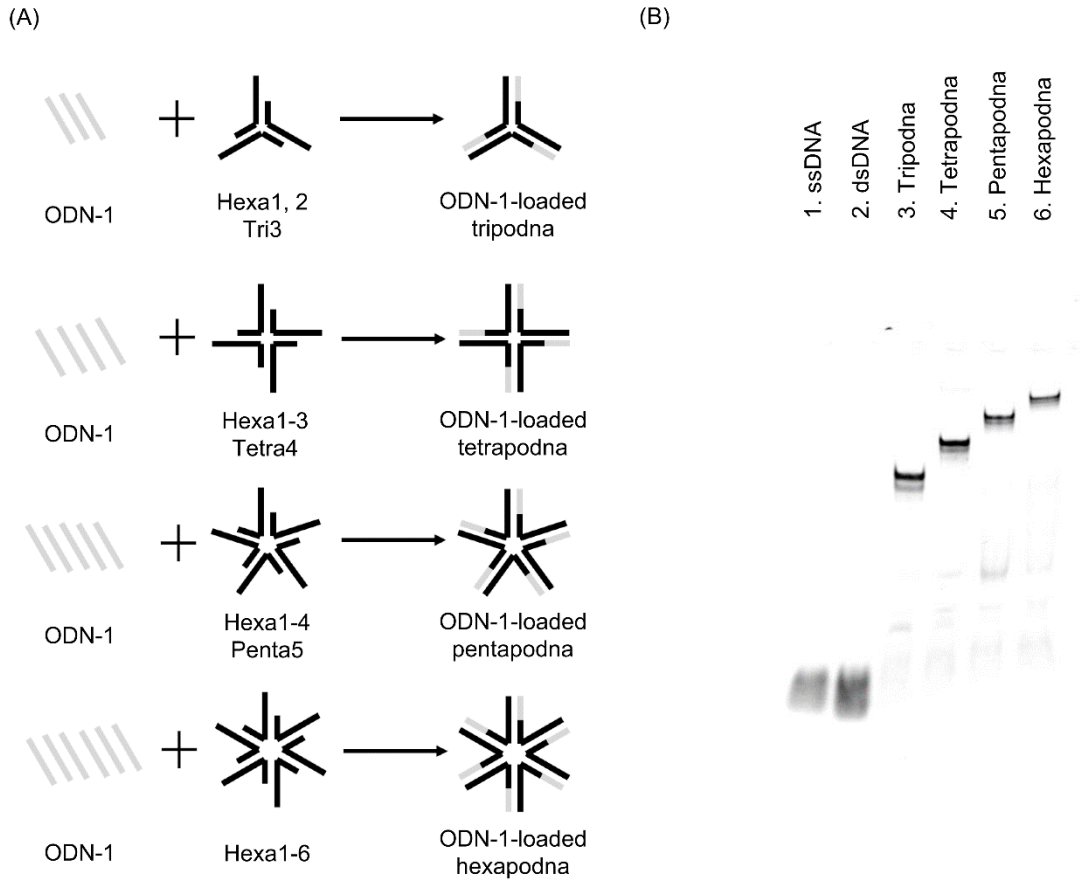

Figure 1. (A) Schematic illustration of the preparation of ODN-1-loaded polypodna. The cases of ODN-1-loaded tripodna, tetrapodna, pentapodna, and hexapodna are shown. (B) PAGE (6%, 37.5:1 acrylamide/bisacrylamide) analysis of polypodna. The gel was run at room temperature (22-25 °C) at 200 V for 20 min in 1 × TBE buffer. The fluorescence by Alexa Fluor 488 of the gel is shown. Lane 1, ssDNA; lane 2, dsDNA; lane 3, tripodna; lane 4; tetrapodna; lane 5, pentapodna; lane 6, hexapodna.

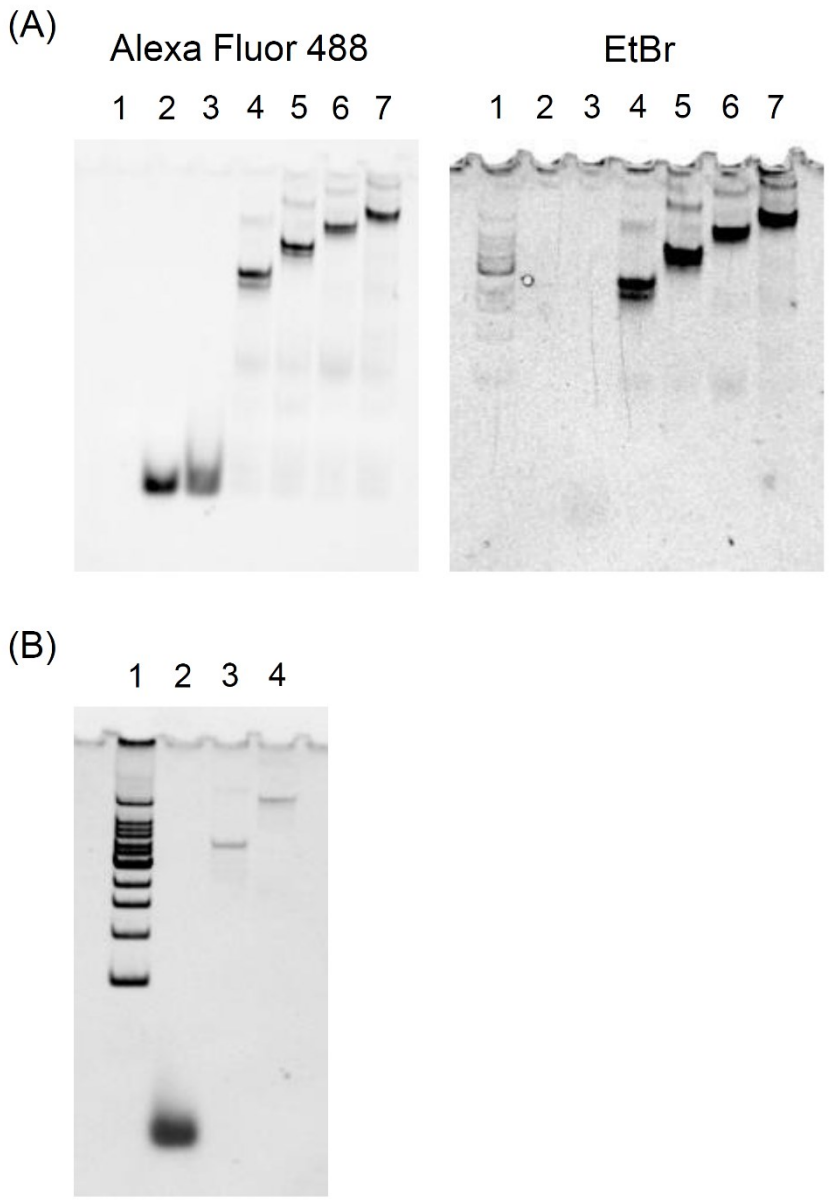

Figure 2. (A) PAGE analysis of polypodna labeled with Alexa Fluor 488. Fluorescence results of Alexa Fluor 488, and ethidium bromide (EtBr) are shown. Lane 1, 100 bp ladder; lane 2, ssDNA; lane 3, dsDNA; lane 4, tripodna; lane 5; tetrapodna; lane 6, pentapodna; lane 7, hexapodna. (B) PAGE analysis of biotinylated polypodna used in this study. The gel was stained by SYBR Gold, and its fluorescence is shown. Lane 1, 100 bp ladder; lane 2, ssDNA; lane 3, tetrapodna; lane 4, hexapodna.

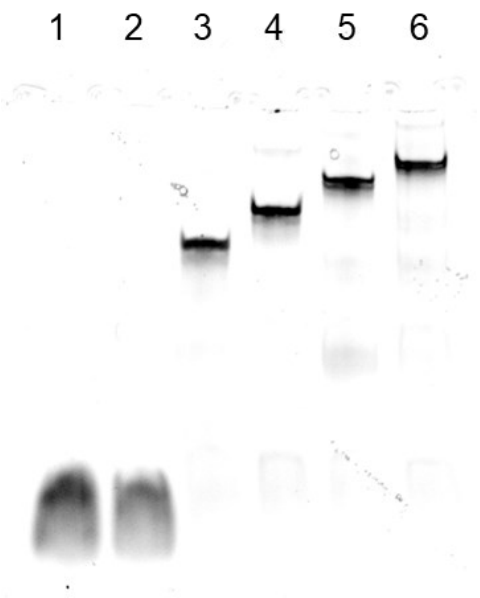

Figure 3. PAGE analysis of polypodnas after incubation with RAW 264.7 cells. Alexa Fluor 488-labeled ssDNA, dsDNA, tripodna, tetrapodna, pentapodna, and hexapodna were incubated with RAW264.7 cells for 2 h at 37 °C. After incubation, culture medium was collected and analyzed by 6% PAGE (22-25 °C, 200 V for 20 min). Fluorescence of Alexa Fluor 488 in the gel was detected. Lane 1, ssDNA; lane 2, dsDNA; lane 3, tripodna; lane 4, tetrapodna; lane 5, pentapodna; lane 6, hexapodna.

1.3.2. Polypodnas were more efficiently crosslinked to MSR1 compared to ssDNA.

Figure 4A shows how the proteins crosslinked with biotinylated DNA were pulled down using streptavidin magnetic beads. Biotinylated ODN-1 (ssDNA), biotinylated ODN-1-loaded tetrapodna, or hexapodna was added to RAW264.7 cells and they were crosslinked with membrane proteins using PFA. Figure 4B shows the western blotting of the collected proteins, using an anti-MSR1 antibody. The bands were detected in the lysates of the cells added with biotinylated ODN-1-loaded tetrapodna and hexapodna. In contrast, almost no bands were detected in the cell lysates after addition of biotinylated ODN-1 (ssDNA). The MSR1 bands were detected in lanes of all the DNA samples, but the band intensity was the highest for hexapodna (Figure 5). Similar results were obtained when murine peritoneal macrophages and BMDCs of BALB/c mice were used instead of RAW264.7 cells (Figure 4C and 4D). When RAW264.7 cells were preincubated with dextran sulfate, a competitive inhibitor of scavenger receptors, no bands were detected in the lysates after addition of hexapodna (Figure 4E), indicating that pull-down of MSR1 reflected efficient interaction of polypodna with MSR1.

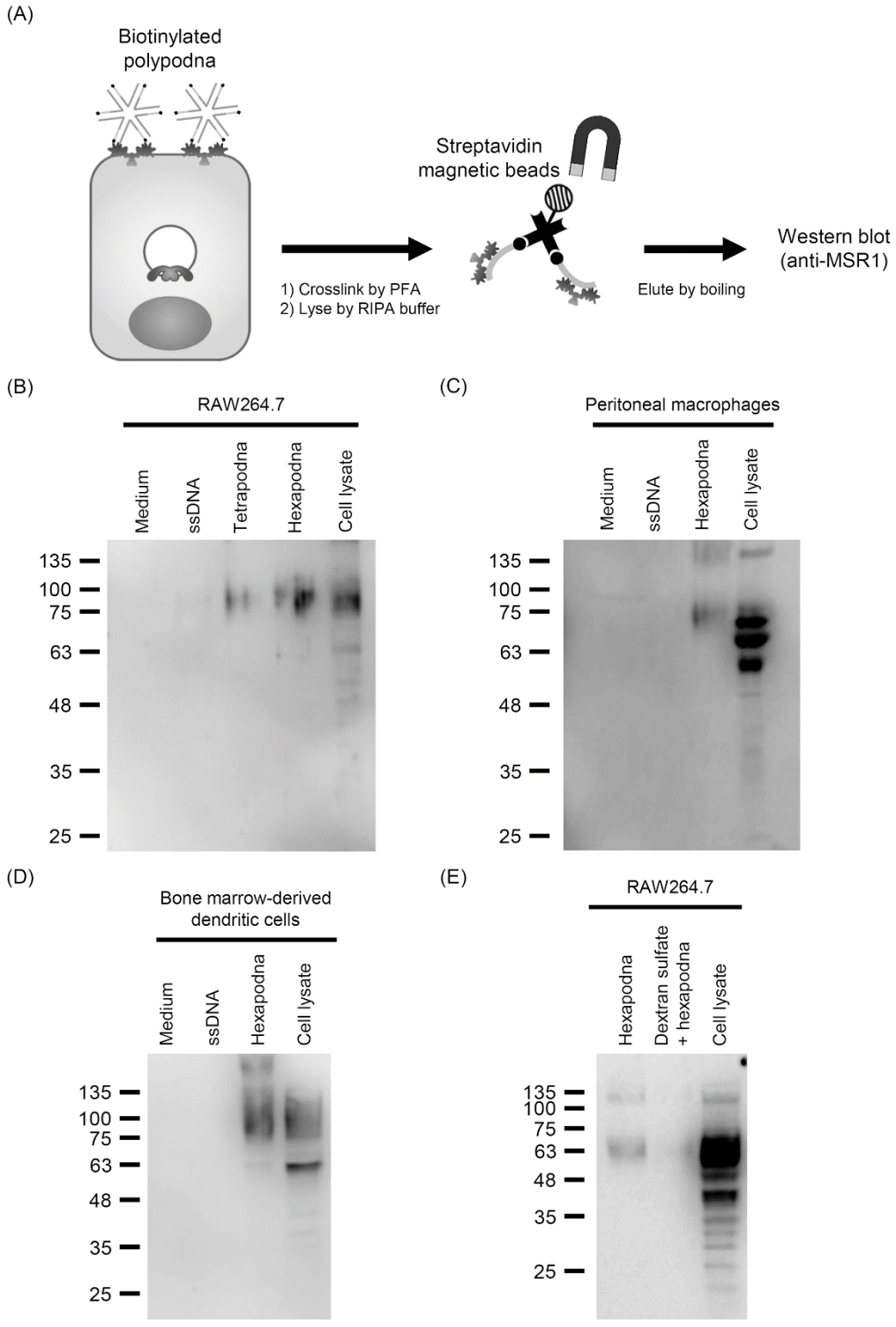
(A)
Biotinylated polypodna
Streptavidin magnetic beads
1) Crosslink by PFA
2) Lyse by RIPA buffer
Elute by boiling
Western blot (anti-MSR1)
(B)
RAW264.7
Medium
ssDNA
Tetrapodna
Hexapodna
Cell lysate
135
100
75
63
48
35
25
(C)
Peritoneal macrophages
Medium
ssDNA
Hexapodna
Cell lysate
135
100
75
63
48
35
25
(D)
Bone marrow-derived dendritic cells
Medium
ssDNA
Hexapodna
Cell lysate
135
100
75
63
48
35
25
(E)
RAW264.7
Hexapodna
Dextran sulfate + hexapodna
Cell lysate
135
100
75
63
48
35
25

Figure 4. (A) Workflow of PFA crosslinking and pull-down of crosslinked proteins. (B, C and D) Western blotting analysis of MSR1 in the proteins crosslinked with biotinylated ssDNA and polypodna. Biotinylated DNAs were added to (B) RAW264.7 cells, (C) peritoneal macrophages and (D) BMDCs obtained from BALB/c mice, and they were crosslinked with PFA. Crosslinked membrane proteins were pulled down using streptavidin magnetic beads. MSR1 in the pulled-down proteins was detected by western blotting. The cell lysate was also analyzed as a positive control.

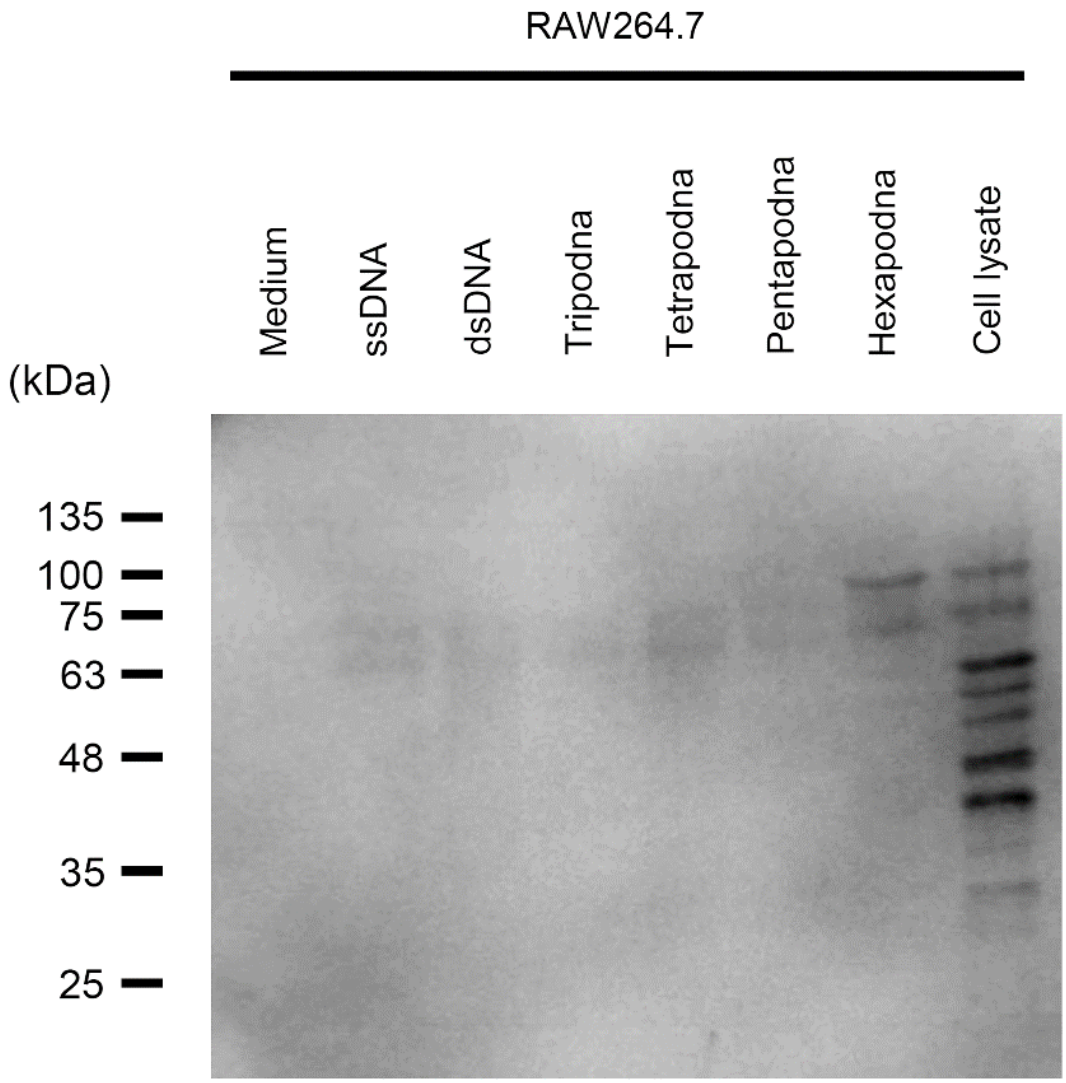

Figure 5. Comparison of the interaction of ssDNA, dsDNA, and each polypodna with MSR1. Biotinylated DNAs were added to RAW264.7 cells, and they were crosslinked with PFA, followed by pull-down by streptavidin magnetic beads. MSR1 in the pulled-down proteins was detected by western blotting.

1.3.3. MSR1-transfection to HEK-Blue hTLR9 cells increased the cellular uptake of polypodna.

To compare the contribution of MSR1 to the cellular uptake of DNA with varying structures, *MSR1*-transfected HEK-Blue hTLR9 cells were prepared.[44] In the previous report, we confirmed that mock-transfection did not alter the cellular uptake of DNA nanostructures,[44] and I used non-transfected cells as a control in this study. Figure 6 shows the cellular uptake of Alexa Fluor 488-labeled ODN-1 (ssDNA) and polypodna loaded with Alexa Fluor 488-labeled ODN-1 by non-transfected and *MSR1*-transfected HEK-Blue hTLR9 cells. The MFI values of non-transfected HEK-Blue hTLR9 cells were low, and the uptake of Alexa Fluor 488-labeled polypodna was significantly higher in MSR1-transfected cells compared with that of non-transfected cells. The MFI values of MSR1-transfected cells were dependent on the structure of the DNA, with the highest for hexapodna, followed by pentapodna, tetrapodna, tripodna, dsDNA, and ssDNA.

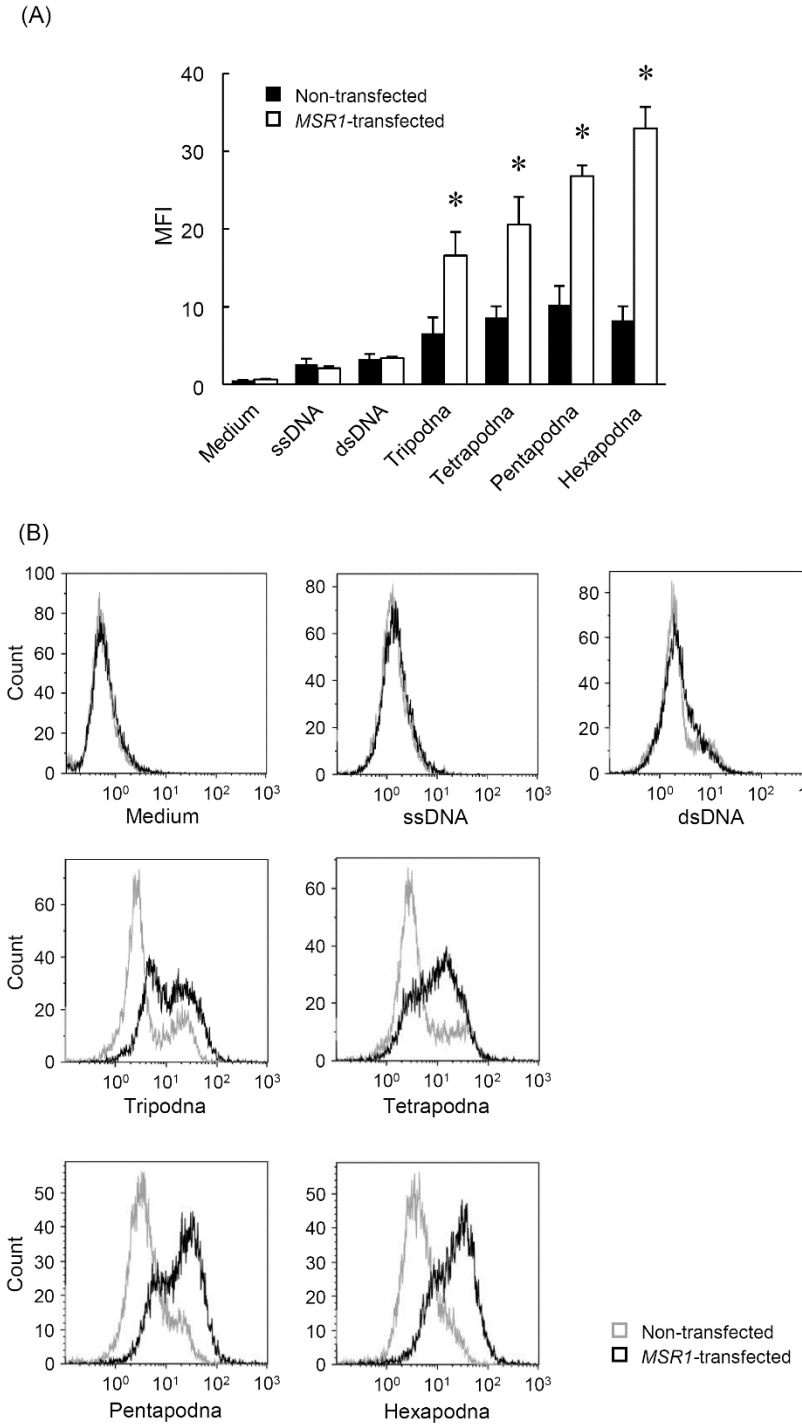

Figure 6. Cellular uptake of Alexa Fluor 488-labeled ssDNA, dsDNA, tripodna, tetrapodna, pentapodna, and hexapodna by non-transfected and *MSR1*-transfected HEK-Blue hTLR9 cells. The cells were incubated with 0.5 μM of Alexa Fluor 488-labeled ODN-1 or polypodna for 2 h, and analyzed by flow cytometry. (A) MFI values were calculated. The results are expressed as mean + SD (n = 4). **P* < 0.05 compared with the non-transfected group. (B) Representative histograms are shown.

1.3.4. Msr1-knockout reduced the cellular uptake of polypodna by RAW264.7 cells.

Figure 7 shows the western blotting of cell lysates of wild-type and 3 *Msr1*-knockout RAW264.7 clones detected using an anti-MSR1 polyclonal antibody and an anti-GAPDH monoclonal antibody. The bands of MSR1 were detected in wild-type RAW264.7 cells (Figure 7, lanes 1), but not in 3 *Msr1*-knockout RAW264.7 cells (Figure 7, lanes 2–4), indicating successful knockout of the *Msr1* gene. The bands of GAPDH were also detected as a loading control. The knockout cell clone in lane 2 was used for the subsequent experiments. Figure 8A and 8B show the results of flow cytometric analysis of wild-type (untreated) and *Msr1*-knockout RAW264.7 cells after addition of Alexa Fluor 488-labeled DNA. The knockout hardly affected the uptake of Alexa Fluor 488-labeled ssDNA. In contrast, the knockout significantly reduced the uptake of Alexa Fluor 488-labeled polypodnas, although the MFI values increased as the number of pods increased. The greatest reduction was observed with Alexa Fluor 488-labeled hexapodna.

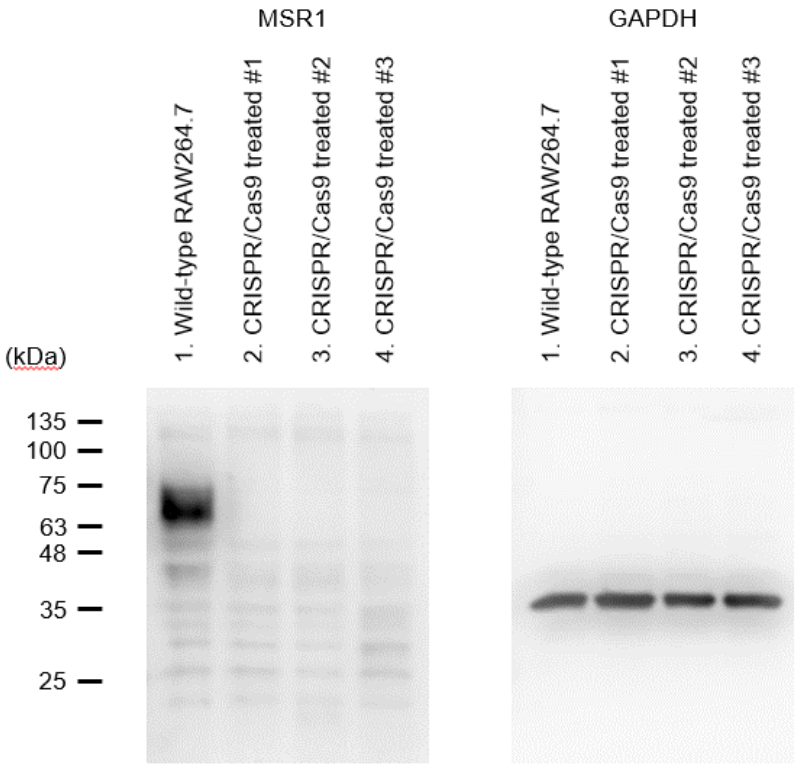

Figure 7. Western blotting analysis of MSR1 in *Msr1*-knockout RAW264.7 cells. The cell lysates of wild-type and *Msr1*-knockout RAW264.7 cells were analyzed by western blotting using polyclonal anti-mouse MSR1 antibody. Lane 1, wild-type RAW264.7 cells; lane 2–4, *Msr1*-knockout RAW264.7 cells. MSR1 bands were not detected in the lanes 2, 3, and 4, indicating successful knockout of *Msr1*. A monoclonal anti-mouse GAPDH antibody was also used as a loading control of cell lysate.

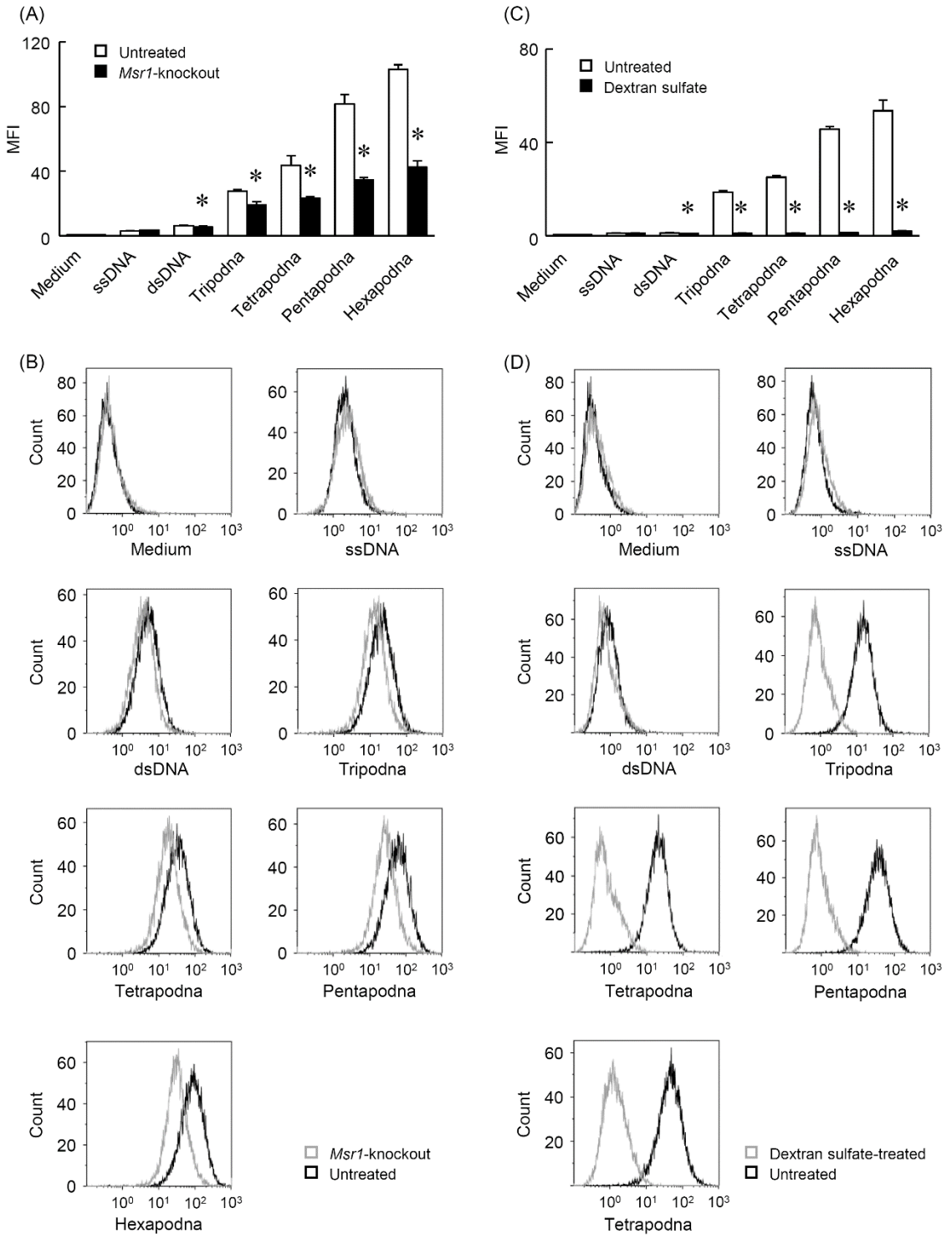

Figure 8. Cellular uptake of Alexa Fluor 488-labeled ssDNA, dsDNA, tripodna, tetrapodna, pentapodna, and hexapodna by (A and B) wild-type (untreated) or *Msr1*-knockout RAW264.7 cells and (C and D) untreated and dextran sulfate-treated RAW264.7 cells. (A and C) The results are expressed as mean + SD (n = 4). **P* < 0.05 compared with the untreated group. (B and D) Representative histograms of (A) and (C) are shown, respectively.

1.3.5. Dextran sulfate reduced the cellular uptake of polypodna by RAW264.7 cells.

Dextran sulfate is an anionic macromolecule and one of the ligands of MSR1 and other scavenger receptors. To confirm the involvement of scavenger receptors including MSR1 in uptake, the uptake of Alexa Fluor 488-labeled DNA was examined using RAW264.7 cells pretreated with dextran sulfate. Figure 8C and 8D show the flow cytometric analysis after addition of each DNA. The treatment with dextran sulfate hardly affected the uptake of Alexa Fluor 488-labeled ssDNA, whereas it significantly reduced the uptake of Alexa Fluor 488-labeled dsDNA and polypodnas.

1.3.6. Msr1-knockout reduced TNF-α release from RAW264.7 cells.

ODN-1 contains the optimal rodent unmethylated CpG motif (GACGTT) and can trigger immunostimulatory cytokine release through the TLR9-signaling. Cytokine release by stimulation of TLR9 reflects on cellular uptake and trafficking to endosomes of CpG DNA because TLR9 expresses within endosomes of macrophages and dendritic cells.[46] Figure 9A and 9B show TNF-α release from wild-type and *Msr1*-knockout RAW264.7 cells after addition of each DNA. PS ODN 1668 (a TLR9 agonist) and lipopolysaccharide (a TLR4 agonist) were used as positive controls. The knockout almost truncated TNF-α release when polypodnas were added to the cells (Figure 9A). In contrast, the knockout hardly affected TNF-α release from the cells when the cells were treated with PS ODN 1668 or lipopolysaccharide (Figure 9B), indicating that the reduced TNF-α release after addition of polypodnas could be attributed to the *Msr-1*-knockout.

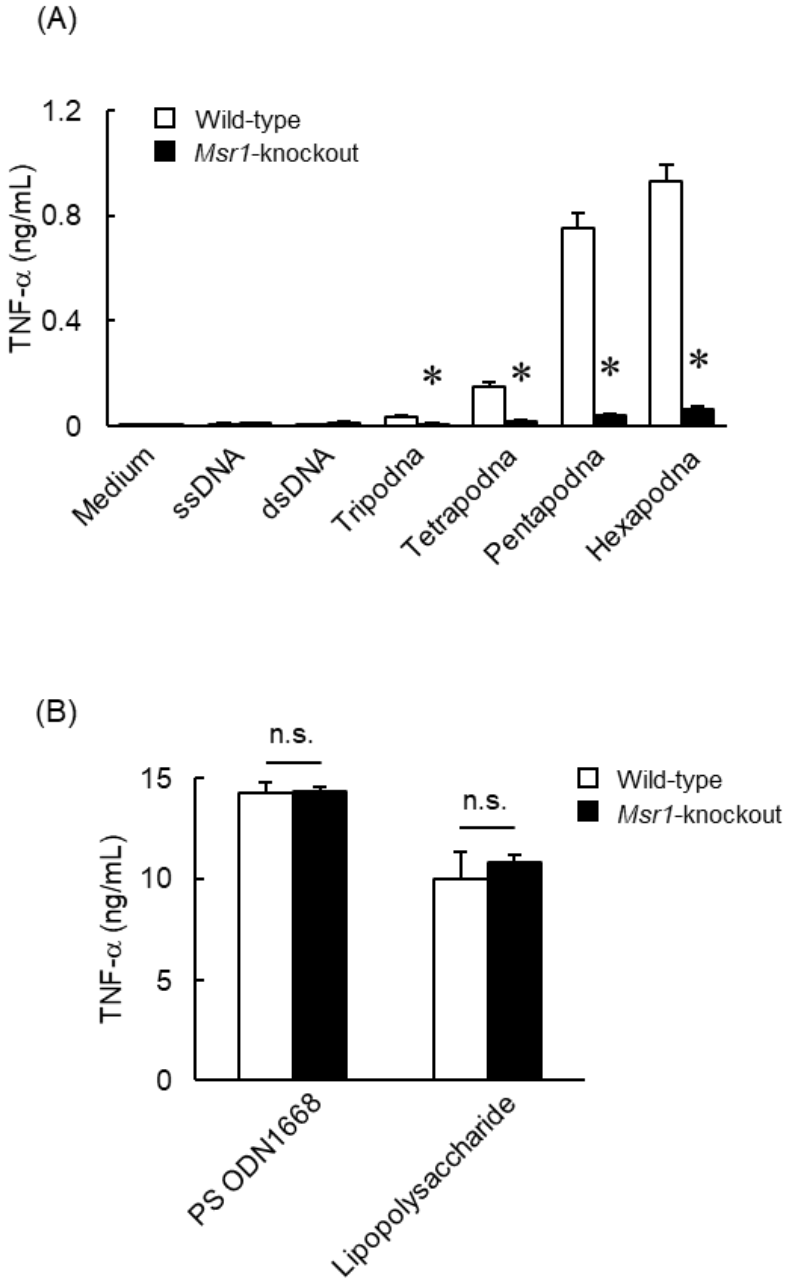

Figure 9. TNF-α release from wild-type or *Msr1*-knockout RAW264.7 cells after addition of (A) ssDNA, dsDNA, tripodna, tetrapodna, pentapodna, and hexapodna, or (B) PS ODN 1668 or lipopolysaccharide. The results are expressed as mean + SD (n = 4). **P* < 0.05 compared with the untreated group.

1.4. Discussion

Previous studies of our group reported that ODNs can be self-assembled to form DNA nanostructures, including polypodnas.[32–34,44] In these experiments, secondary faint bands were sometimes detected in PAGE. In the present study, I also found such secondary faint bands (Figure 1-3), which could be incomplete or more complicated DNA nanostructures. However, PAGE showed that the formation efficiency of polypodnas was high enough for use in experiments.

Previous reports showed that branched DNA nanostructures were more efficiently taken up by immune cells compared with that of linear ssDNA and dsDNA. Importantly, this efficient uptake was found to be cell type-specific, suggesting the involvement of cell surface receptors for the uptake of such branched DNA nanostructures. Immune cells take up and remove pathogen-associated molecular patterns (PAMPs) and damage-associated molecular patterns (DAMPs), and express endocytic receptors for PAMPs/DAMPs.[47,48] PAMPs/DAMPs include extracellular DNA derived from bacteria and necrotic cells; therefore, there is a possibility that DNA nanostructures are taken up by immune cells through the same mechanisms as PAMPs/DAMPs.

Previous studies by other groups have reported that several membrane proteins, including MAC-1, AGER, MNAB, DEC-205, and MRC1 are involved in the cellular uptake of DNA.[36–41] However, preliminary studies of our group showed that AGER, MNAB, DEC-205, and MRC1 are not expressed on RAW264.7 cells or murine dendritic cell line DC2.4 cells, suggesting that these receptors are not the receptors of polypodna in these cells. Moreover, the transfection of MAC-1 to HEK-Blue hTLR9 cells hardly increased the uptake of DNA (data not shown). Thus, it is implied that these membrane proteins are not involved in the efficient cellular uptake of DNA nanostructures by immune cells. However, little information is available how each of these receptors contributes to the uptake.

The previous results from our group showed that polypodna more efficiently interacted with RAW264.7 cells or other immune cells, and that efficient uptake was dependent on the pod number.

However, the molecular mechanisms for this phenomenon have remained to be elucidated. Our group also reported that the MSR1 is involved in DNA uptake, but little is known how much MSR1 is responsible for this efficient uptake of DNA nanostructures. The interaction of MSR1 with its ligands was studied, and the positively charged collagen-like domain of MSR1 was revealed to be responsible for ligand binding.[49,50] In addition, DNA nanostructures have higher densities of negative charges than ssDNA. Thus, the results in CHAPTER 1 imply that complicated DNA nanostructures, which have a high-density negative charge, could efficiently interact with MSR1, leading to efficient cellular uptake.

Three alternative splicing variants of human MSR1 have been reported.[51,52] The isoform type 1 and 2 internalize negatively-charged macromolecules, whereas the isoform type 3 is a non-functional receptor because it is trapped within endoplasmic reticulum. In the transfection experiments, we used a cDNA clone of human MSR1 encoding isoform type 1, which is a functional isoform. On the other hand, murine MSR1 has two alternative splicing variants, both of which can be functional receptors, according to the UniProt (https://www.uniprot.org/). CRISPR/Cas9 can be a useful tool to confirm whether a protein of interest is involved in the cellular response. CRISPR/Cas9 changes the genome sequence at the target site, and thus truncates any functional *Msr1* mRNA transcripts. The present study demonstrated that the knockout significantly reduced the uptake of polypodnas. Despite the apparent involvement of MSR1 in the cellular uptake of polypodna, the uptake experiment showed that the MFI of *Msr1*-knockout RAW264.7 cells was still significantly higher than that of untreated cells (sample “medium”) (Figure 8). However, *Msr1*-knockout almost completely reduced the cytokine release from the cells (Figure 9). The MFI values did not decrease as much as cytokine release. Considering that TLR9 is expressed in the endosomes and lysosomes,[46] polypodnas need to be delivered to these subcellular compartments to induce cytokine release. The MFI values would reflect not only the cellular uptake or internalization of polypodna, but also the binding to the cell surface. Polypodnas bound to membrane proteins other than MSR1 could not be efficiently internalized and

delivered to the endosomes or lysosomes. These results suggest that polypodna specifically bind to MSR1 as well as nonspecifically to cell surface, and only those bound to MSR1 are efficiently internalized. This interpretation can explain the results showing that *Msr1*-knockout partly reduced the cellular uptake of polypodna, but almost completely abrogated the TNF-α secretion. Thus, it can be concluded that MSR1 plays a dominant role in the uptake of nanostructured DNA.

The results in this chapter consistently show that MSR1 is a key receptor that is involved in the uptake of nanostructured DNA. It can be estimated that DNA nanostructures are well-delivered to MSR1-expressing immune cells. In conclusion, the efficient uptake of nanostructured DNAs by immune cells is mediated by their efficient recognition by MSR1.

CHAPTER 2

Development of unmethylated CpG DNA with long-lasting endosome targeting ability

2.1. Introduction

The development of new adjuvants for human vaccines with potent and long-lasting immune response has been widely studied. However, there are still limitations in immune responses and toxicities for the clinical application of adjuvants.[53]

Unmethylated CpG motifs are potent immunostimulatory activators via pattern recognition-triggered immune response, and have been studied as vaccine adjuvants and cancer immunotherapies.[54–56] CpG motifs are derived from bacterial and viral genomes and classified as PAMPs.[48] CpG motifs can be specifically recognized by TLR9 expressed in the endosomes of immune cells such as macrophages and dendritic cells.[46] This recognition initiates the expression of proinflammatory cytokines (e.g. TNF-α, IL-6) and chemokines (e.g. CXCL9, CXCL13) to promote innate and adaptive immune responses.[57,58] CpG DNA is expected to be used as therapeutics against various diseases including cancers, allergies, and infectious diseases,[59,60] and Heplisav-B was approved as a vaccine containing CpG DNA adjuvant for hepatitis B.[61] Nevertheless, naked CpG DNA is easily degraded by DNase, and is poorly taken up by immune cells due to the electrostatic repulsion between the negatively charged DNA and the electronegative cell surface.[62,63] To develop functional CpG adjuvants, it is required to deliver CpG DNA to endosomes and to avoid degradation by DNase.

Rolling circle amplification (RCA) is an isothermal nucleic acids amplification strategy that produces long single-stranded DNA (lssDNA) with periodic sequences from a circle template DNA.[64] LssDNA has higher density of negative charges than short ODNs. Based on the results in CHAPTER 1, it could be taken up by efficient recognition of MSR1. Previous reports by other groups showed that nanoparticles synthesized by RCA containing CpG motifs have shown to be easily taken up by macrophages and subsequently induced proinflammatory cytokines.[57,65] Meanwhile, our group reported that lssDNA-containing nanoparticles, as well as short ODNs, are prone to nuclease degradation and lack the ability of long-lasting cytokine induction.[22] Therefore, I hypothesize

retarding the degradation of lssDNA would lead to the development of a potent and effective CpG adjuvant. Chemical modification, which was applied to Heplisav-B as well, is not compatible to lssDNA-producing polymerase.

An i-motif is a quadruplex DNA structure based on cytosine and protonated cytosine ($C\text{-}C^+$) intercalated base pairs and its formation is highly pH-dependent.[66] At slightly acidic pH, i-motifs fold into a quadruplex structure. When changing the pH to neutral condition, the i-motif structures are unfolded and reversibly return to the single linear strands.[67] An i-motif structure is formed from four or two strands (intermolecularly) and one strand (intramolecularly) with cytosine stretches. Recently, i-motifs have been studied in the DNA nanotechnology field.[67] For instance, it was reported by other groups that DNA hydrogel could be synthesized by RCA, utilizing i-motifs.[68]

Here, I hypothesized that DNA hydrogel would avoid degradation by DNase. Endosomes are acidic,[69,70] and therefore, i-motif-containing lssDNA would form hydrogels within endosomes after the cellular uptake. In CHAPTER 2, I attempted to design a DNA nanostructure which induces long-lasting stimulation of TLR9 by introducing intermolecular i-motifs and CpG motifs to lssDNA synthesized by RCA. I expected that, when taken up into the acidic endosome of immune cells, lssDNA containing i-motifs turns to form intermolecular i-motif structures between DNA chains and a three-dimensional hydrogel network, leading to the protection of DNA from enzymatic degradation in endosome, which would result in strong, durable, and sustainable stimulation of TLR9 (Figure 10).

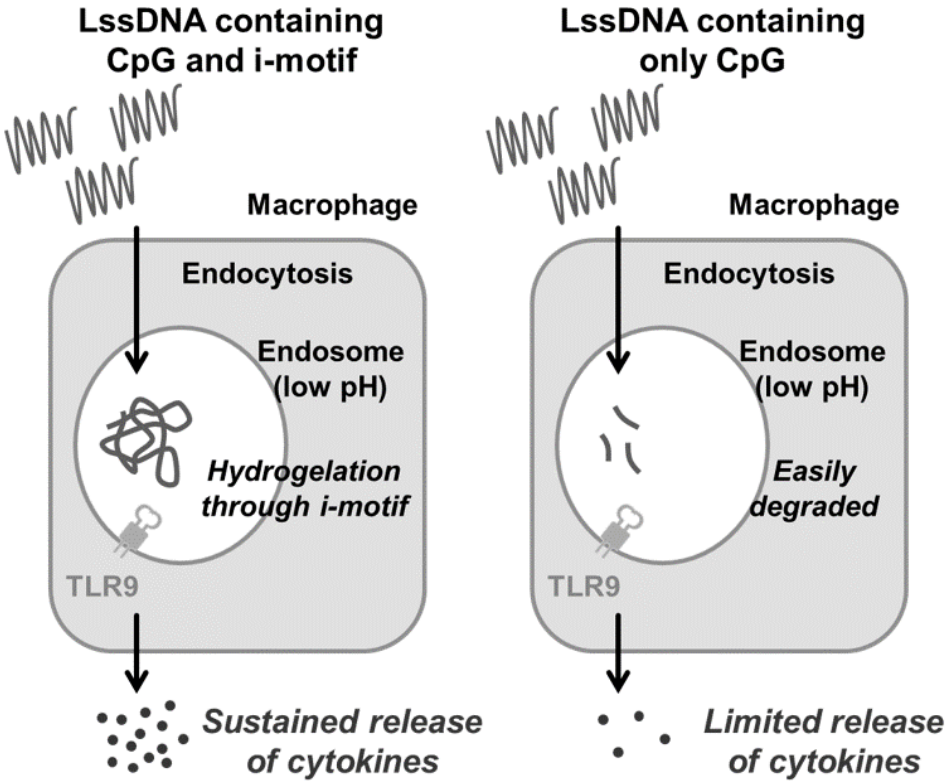

Figure 10. Schematic illustration of i-motif- and CpG motif-containing lssDNA. After the cellular uptake of lssDNA, low pH of endosomes promotes conformational changes of lssDNA through i-motifs, resulting in hydrogelation. LssDNA hydrogels are expected to stimulate TLR9 for a longer period of time, which leads to sustained release of cytokines from immune cells.

2.2. Materials & Methods

2.2.1. Chemicals

All chemicals were of the highest grade available and used without further purification, described in CHAPTER 1 as well.

2.2.2. Animals

Six-week-old male C57BL/6J mice were purchased from Japan SLC, Inc. The protocols for all the animal experiments were approved by the Animal Experimentation Committee of the Graduate School of Pharmaceutical Sciences, Kyoto University.

2.2.3. Cells

RAW264.7 cells (murine macrophage-like cells) were purchased and cultured as described in CHAPTER 1.

2.2.4. ODNs

All ODNs were obtained from FASMAC Co., Ltd. (Kanagawa, Japan). Sequences of the ODNs used are shown in Table 3.

Table 3. Sequences of the ODNs used in this study.

Name	Sequences (5′ → 3′)
i_1-CpG-monomer	GAGACGTTCTCACCGAATGCTTGAA **CCCTCCCTCCCTCCC** GACTGCAAGT
i_2-CpG-monomer	GAGACGTTCTCACCGAATGCTTGAA **CCCCCTCCCCC** GACTGCAAGT
i_3-CpG-monomer	GAGACGTTCTCACCGAATGCTTGAA **CCCCCCTCCCCCC** GACTGCAAGT
i_4-CpG-monomer	GAGACGTTCTCACCGAATGCTTGAA **CCCCCTTTCCCCC** GACTGCAAGT
CpG-monomer	GAGACGTTCTCACCGAATGCTTGAA TTTTTTTTTTTTT GACTGCAAGT
CpG 1668	TCCATGACGTTCCTGATGCT
i_2-CpG-lssDNA template	ACTTGCAGTC GGGGGAGGGGG TTCAAGCATTCGGTG AGAACGTCTC
i_3-CpG-lssDNA template	ACTTGCAGTC GGGGGGAGGGGGG TTCAAGCATTCGGTG AGAACGTCTC
CpG-lssDNA template	ACTTGCAGTC AAAAAAAAAAAAA TTCAAGCATTCGGTG AGAACGTCTC
Primer for CpG-lssDNAs	GACTGCAAGTGAGACGTTCT
i_2-GpC-lssDNA template	ACTTGCAGTT GGGGGAGGGGG TTCAAGCATTGGCTG AGAAGCTCTC
i_3-GpC-lssDNA template	ACTTGCAGTT GGGGGGAGGGGGG TTCAAGCATTGGCTG AGAAGCTCTC
GpC-lssDNA template	ACTTGCAGTT AAAAAAAAAAAAA TTCAAGCATTGGCTG AGAAGCTCTC
Primer for GpC-lssDNAs	AACTGCAAGTGAGAGCTTCT

Bold faces in i_x-CpG monomers (x = 1, 2, 3, and 4) are the sequences that form i-motif structures. The underlined parts of lssDNA templates are complementary to each primer. All of the ODNs, including CpG 1668, are phosphodiester DNA. Repeated sequences complementary to the lssDNA templates were synthesized by RCA.

2.2.5. PAGE analysis

The i-motif-forming behaviors were investigated by using 10% native PAGE. ODNs with different types of i-motifs, i_x-CpG-monomers (x = 1, 2, 3, and 4), and the control CpG-monomer were used for the characterization. Each ODN (20 μM) dissolved in pH 5.0 or pH 7.4 Tris/AcOH buffer (40 mM) were heated at 95 °C for 10 min, and then gradually cooled to 4 °C. Gel electrophoresis was performed in the corresponding Tris/AcOH buffer (40 mM) of pH 5.0 or pH 7.4 for 40 min at 4 °C (under a voltage of 250 V). Finally, the gels were stained with SYBR Gold for 30 min.

The upper bands which showed low electrophoretic mobility at pH 5.0 were regarded as multimolecular i-motif structure generated by the intermolecular i-motif formation. Based on this assumption, intermolecular i-motif forming ratio (%) was calculated by the fluorescence intensities (*FI*) using the following formula:

$$Intermolecular\ i\text{–}motif\ ratio\ (\%) = \frac{FI_{upper\ band}}{FI_{upper\ band} + FI_{lower\ band}} \times 100$$

2.2.6. RCA reaction

There are three steps in an RCA reaction. 1) Annealing: LssDNA template (10 μM) was mixed with its primer (10 μM) in annealing buffer (10 mM Tris-HCl [pH 8], 1 mM ethylenediaminetetraacetic acid (EDTA), and 200 mM NaCl). After being heated at 95 °C for 5 min, the mixture was gradually cooled to 20 °C. 2) Ligation: The annealed template–primer hybrid was mixed with 10 U/μL T4 DNA ligase (Takara Bio Inc.) and T4 DNA ligase buffer (66 mM Tris-HCl [pH 7.6], 6.6 mM $MgCl_2$, 10 mM dithiothreitol (DTT), and 0.1 mM adenosine triphosphate (ATP)), and then ligated at 16 °C overnight. ODNs that were not circularized were removed by enzymatic reaction using 25 U/mL exonuclease I (Takara Bio Inc.) and 1000 U/mL exonuclease III (Takara Bio Inc.) at 37 °C for 1 h. To purify circularized DNAs, the reaction mixture was mixed with the same volume of phenol:chloroform:isoamyl alcohol (25:24:1) (Nacalai Tesque), shaken for 5 min at room

temperature, and centrifuged at 15,000 *g* for 10 min. The upper fraction was collected, followed by ethanol precipitation as shown later. 3) Amplification: The ligated circular single-stranded DNA (10 μM) and primer DNA (10 μM) were mixed in the annealing buffer and annealed by heating at 95 °C for 5 min, followed by gradual cooling to 20 °C. The mixed solution was incubated with 0.2 U/μL phi29 DNA polymerase (Lucigen, WI), 50 mM Tris-HCl [pH 7.5], 10 mM $MgCl_2$, 10 mM $(NH_4)_2SO_4$, 4 mM DTT, 200 μg/mL BSA, 2 mM of each dNTP (Invitrogen, Carlsbad, CA) at 30 °C for 24 h, and then the mixture was heated at 80 °C for 10 min to deactivate the DNA polymerase. The highly viscous RCA product was heated to 95 °C for 10 min in 83.5 mM EDTA to solubilize the product.

2.2.7. Ethanol precipitation

DNA was precipitated in ethanol for its purification from contaminants. Solution with DNA was diluted by ethanol (70% as final concentration) and sodium acetate (AcONa) solution (135 mM as final concentration), and 20 μg of glycogen was added. After mixing them for 1 min, it was incubated for 1 h at -20 °C, followed by centrifugation at 15,000 *g* for 20 min. The supernatant was discarded, and the pellet was washed by 300 μL of 70% ethanol, followed by centrifugation at 15,000 *g* for 3 min. The supernatant was discarded again, and the pellet was dried under reduced pressure for use in subsequent experiments.

2.2.8. Agarose gel electrophoresis

The lssDNA samples in pH 5.0 or pH 7.4 Tris/AcOH buffer (40 mM) were incubated at 20 °C for 30 min. Samples were loaded onto 0.6% agarose gel, and gel electrophoresis was performed in the corresponding Tris/AcOH buffer (40 mM) of pH 7.4 or 5.0 for 35 min at 4 °C (under a voltage of 100 V). The DNA was stained with SYBR Gold for 30 min for its visualization.

2.2.9. pH-Induced formation of a hydrogel

i_2-CpG-lssDNA, i_3-CpG-lssDNA, and CpG-lssDNA were soaked in 4 μL of buffer (50 mM Tris, 100 mM NaCl, pH 10). Each lssDNA was heated for 5 min at 80 °C to fully unfold the long DNA sequences, and then HCl (0.2 N) was added to adjust the pH to 5.0 and 7.4. Afterwards, the DNA was stained with propidium iodide (PI) (5 mM PI, 150 mM NaCl), and left stand without disturbing until a hydrogel formed. The changes in shape of the DNA hydrogels were recorded with a camera.

2.2.10. TNF-α release from RAW264.7 cells

RAW267.4 cells were plated in 96-well plates at a density of 2×10^4 cells/well prior to treatment. After purification RCA product with NucleoSpin Gel and PCR Clean-up (MACHEREY-NAGEL GmbH & Co., St. Neumann Neander, Duren, Germany), the cells were treated with lssDNAs at a DNA concentration of 15 nM diluted in 100 μL of Opti-MEM for 8 h and 24 h. The amount of TNF-α in the supernatant was analyzed by ELISA using an OptEIA mouse TNF (Mono/Mono) ELISA set (BD Biosciences) in accordance with the manufacturer's protocol.

2.2.11. Induction of cytokines in mice

C57BL/6J mice were intradermally injected with CpG-lssDNAs at a dosage of 13 μg DNA (0.87 nmol/mouse as CpG equivalents). One day and two days after injection, mice were anesthetized with isoflurane, and the injection site and draining inguinal lymph nodes were excised. Total RNA from the injection site and draining lymph nodes were extracted using Sepasol RNA I super G (Nacalai Tesque). The extracted RNA was reverse-transcribed with a ReverTra Ace qPCR RT Kit (TOYOBO Co., Ltd., Osaka, Japan). For quantitative analysis of mRNA expression, real-time PCR was conducted with total RNA using KAPA SYBR FAST ABI Prism 2× qPCR Master Mix (KAPA BIOSYSTEMS, Inc., Boston, MA). Primer sequences are shown in Table 4. Amplified products were detected via

intercalation of SYBR Green, a fluorescent dye, by using StepOnePlus Real Time PCR System (Applied Biosystems, Foster City, CA). The *Il-6* and *Cxcl9* mRNA expression was normalized to the mRNA level of *Gapdh*.

Table 4. Sequences of the primers used for real-time qPCR.

Gene		Sequences (5′ → 3′)
Il-6	Forward	GTTCTCTGGGAAATCGTGGA
	Reverse	TGTACTCCAGGTAGCTATGG
Cxcl9	Forward	CCTAGTGATAAGGAATGCACGATG
	Reverse	CTAGGCAGGTTTGATCTCCGTTC
Gapdh	Forward	AGGTCGGTGTGAACGATTG
	Reverse	TGTAGACCATGTAGTTGAGGTCA

2.2.12. Statistical analysis

Statistical analysis was performed using Student's t-test for comparison between two groups and one-way analysis of variance (ANOVA) followed by Tukey–Kramer tests for comparisons among more than two groups. Differences were considered statistically significant at *P* values less than 0.05.

2.3. Results

2.3.1. Sequences of DNA were optimized for efficient formation of intermolecular i-motif.

Inter- and intramolecular i-motif structures are two possible products of i-motif formation. To obtain DNA hydrogels, it is necessary to construct efficient intermolecular i-motif structures among the RCA products under acidic condition.[68,71] Therefore, four types of i_x-CpG-monomers (x = 1, 2, 3, and 4) containing i-motifs with different patterns of cytosine were newly designed. CpG-monomer whose i-motif sequence was converted to poly dT was prepared as a control.

First, the conformations of the i_x-CpG-monomers at different pH values were investigated by 10% native PAGE (Figure 11). At pH 7.4, only a single band was observed for each sequence and displays an electrophoretic mobility primarily dependent on the molecular weight (Figure 11A). When lowering the pH to 5.0, a large decrease in the electrophoretic mobility was observed, which indicates intermolecular i-motif-dependent conformational changes occurred upon the pH switch (Figure 11B). Based on the fluorescent intensities of bands, intermolecular i-motif forming ratios were calculated. i_2-CpG monomer and i_3-CpG-monomer showed significantly higher intermolecular i-motif forming ratio, compared to i_1- and i_4-CpG-monomers (Figure 11C). Therefore, the i-motif sequences of i_2 and i_3 were used for the following studies.

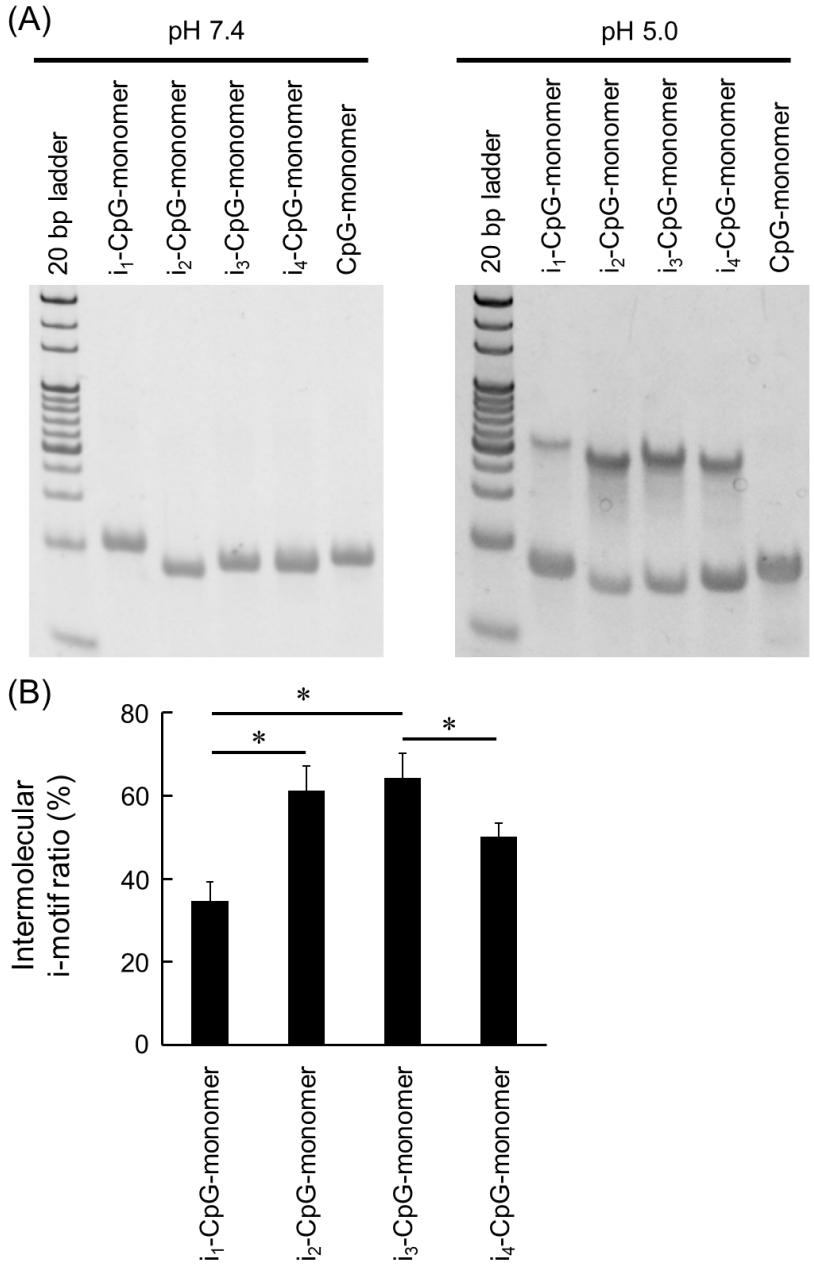

Figure 11. Characterization of i_x-CpG-monomers (x = 1, 2, 3, and 4). (A) PAGE analysis of the i-motif formation of i_x-CpG-monomers at pH 7.4 and pH 5.0. (B) Intermolecular i-motif forming ratios of i_x-CpG-monomers calculated from band intensities. PAGE analysis was conducted independently three times, and the results are expressed as mean + SD (n = 3). *P < 0.05.

2.3.2. Conformational changes of lssDNA by i-motifs were analyzed by electrophoresis.

LssDNAs were synthesized based on the sequences of i_2- and i_3-CpG monomers, and their physical properties were evaluated. Figure 12 shows the conformational changes of the i_2- and i_3-CpG-lssDNA at different pH values. At pH 7.4, i_2- and i_3-CpG-lssDNA and the control CpG-lssDNA showed the bands with almost the same mobilities. When lowering the pH to 5.0, the bands of i_2- and i_3-CpG-lssDNA turned faint, whereas that of CpG-lssDNA was observed. These pH-induced changes of i_2- and i_3-CpG-lssDNA can be attributed to the intermolecular i-motif folding and formation of bulky structures.

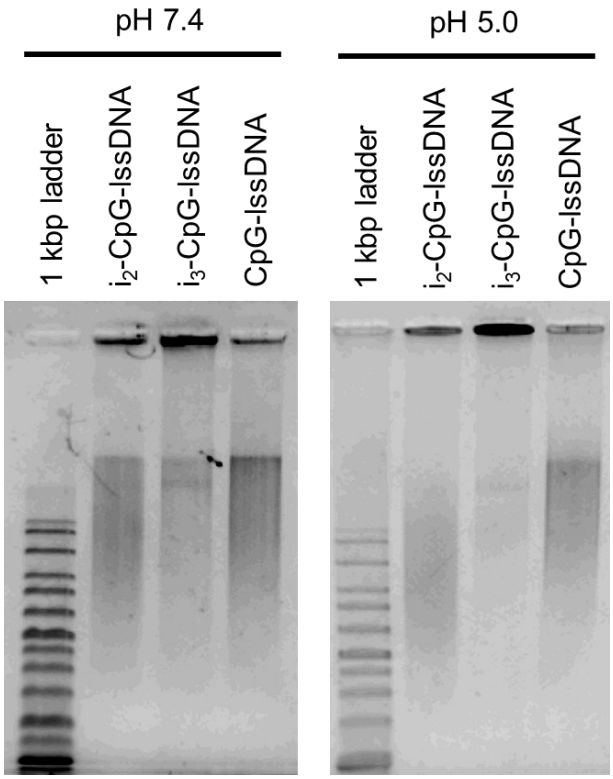

Figure 12. Characterization of i_2- and i_3-CpG-lssDNA. Agarose gel electrophoretic analysis of i_2- and i_3-CpG-lssDNA at pH 7.4 and pH 5.0.

2.3.3. i_3-CpG-lssDNA formed hydrogel at pH5.0.

To investigate whether i_2- and i_3-CpG-lssDNA form hydrogels in acidic conditions, lssDNAs were dissolved to buffers of pH 8.0 and 5.0, and the state of the solution was observed. To visualize lssDNA, it was stained by propidium iodide (PI), which intercalates in DNA strands. Figure 13A shows each lssDNA stained with PI. In pH 8.0, lssDNA dissolved in buffer to be clear solutions. In pH 5.0, however, i_3-CpG-lssDNA changed to be like aggregates. In addition, Figure 13B shows each lssDNA in pH 5.0 buffer when aspirating it with a micropipette. i_3-CpG-lssDNA could not be aspirated because of high viscosity whereas i_2-CpG-lssDNA and CpG-lssDNA were easily aspirated. These results suggested the formation of hydrogel of i_3-CpG-lssDNA only in pH 5.0.

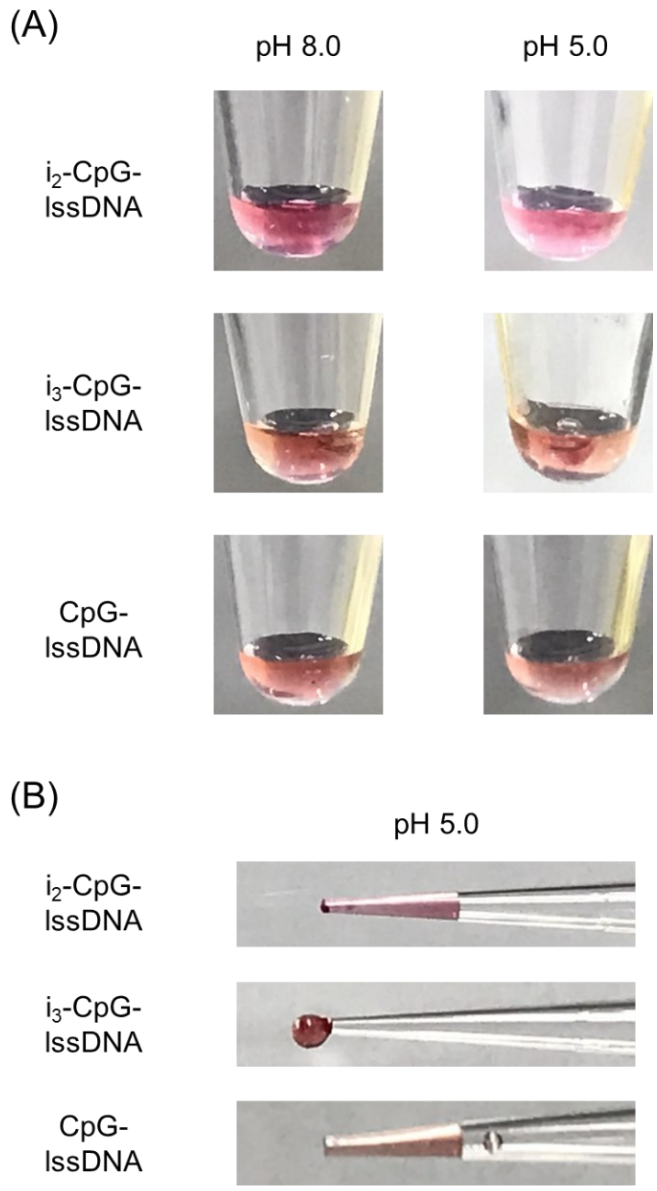

Figure 13. i-Motif-containing lssDNA in pH 8.0 and pH 5.0 buffers. (A) Images of each lssDNA dissolved in pH 8.0 and pH 5.0 buffers. i_3-CpG-lssDNA formed aggregates only in pH 5.0. (B) Images of lssDNA removed from a tube on a pipette tip. i_3-CpG-lssDNA in pH 5.0 could not be aspirated due to its high viscosity.

2.3.4. i_3-CpG-lssDNA induced sustained release of TNF-α from RAW264.7 cells.

The immunological effects of i_2- and i_3-CpG-lssDNA *in vitro* were examined by measuring the amount of TNF-α released from RAW264.7 cells. TNF-α was measured 8 h and 24 h after addition of each lssDNA (Figure 14). After 8 h, i_2- and i_3-CpG-lssDNA significantly induced higher amount of TNF-α than CpG-lssDNA, but the low concentration of CpG DNA (15 nM) limited the release of TNF-α in low levels. However, 24 h after addition of lssDNA, higher amount of TNF-α was secreted by i_3-CpG-lssDNA than by CpG-lssDNA. These results suggested that i_3-CpG-lssDNA induced sustained cytokine production.

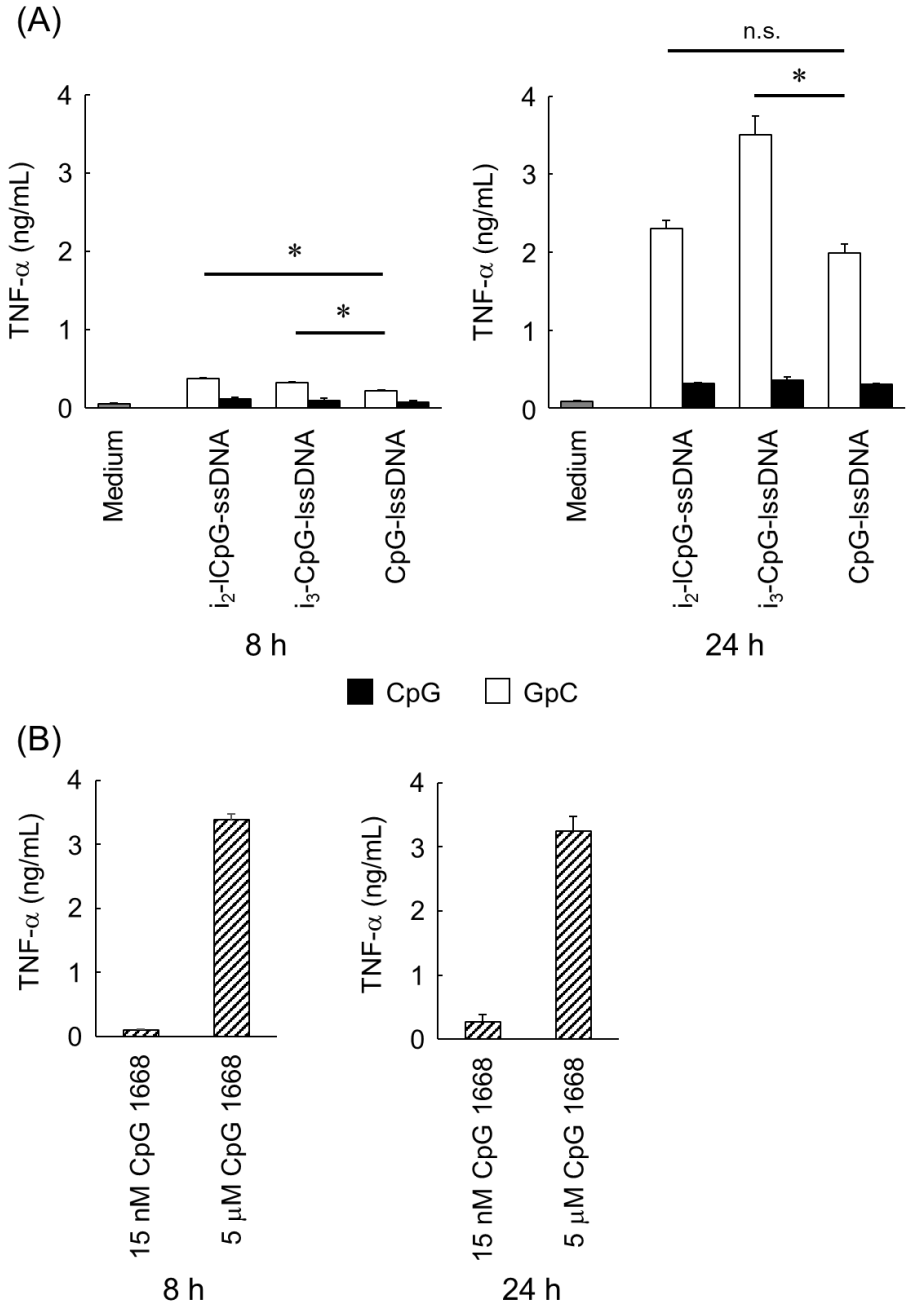

Figure 14. The levels of released TNF-α from RAW264.7 cells treated for 8 h and 24 h. (A) RAW264.7 cells were treated with each CpG- and GpC-lssDNA. LssDNAs were diluted in Opti-MEM at the concentration of 15 nM as CpG or GpC sequences. (B) RAW264.7 cells were treated with phosphodiester CpG 1668 ODNs at the concentration of 15 nM or 5 μM. The results are shown as mean + SD (n = 4). **P* < 0.05.

2.3.5. Intradermal administration of i_3- CpG lssDNA induced higher Il-6 in the lymph nodes of mice.

Lastly, I evaluated the immunostimulatory properties of i_3-CpG-lssDNA *in vivo*. i_3-CpG-lssDNA and CpG-lssDNA were intradermally injected to C57BL/6J mice. The injection site and draining lymph nodes were collected 1 day and 2 days after injection. Figure 15 shows the relative amount of mRNA of *Il-6* and *Cxcl9*. At the draining lymph node 2 days after injection, the expression of *Il-6* significantly increased by i_3-CpG-lssDNA compared to CpG-lssDNA. In addition, i_3-CpG-lssDNA was more likely to induce both *Il-6* and *Cxcl9* at the injection site. These results indicated that i_3-CpG-lssDNA continuously activated immune systems via sustained stimulation of TLR9.

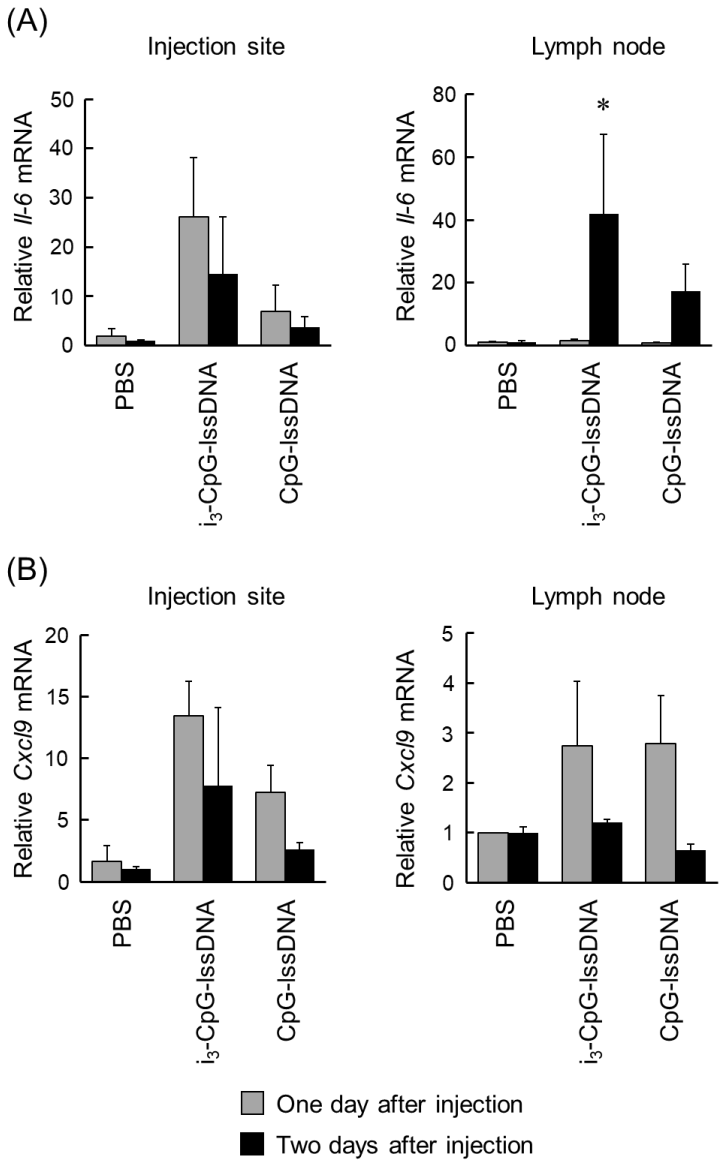

Figure 15. Upregulation of *Il-6* and *Cxcl9* mRNA expression by i_3-CpG-lssDNA. C57BL/6J mice were intradermally injected with PBS, i_3-CpG-lssDNA, and the injection site and the draining lymph node was collected, and quantified mRNA of (A) *Il-6* and (B) *Cxcl9* one day and two days after injection. mRNA amounts relative to PBS-administered mice on one day after injection are shown as mean + SD (n = 3). **P* < 0.05 compared with CpG-lssDNA-administered mice on the same day.

2.4. Discussion

In this chapter, I demonstrated the development of functionalized DNA containing CpG motifs that changed its conformation through intermolecular i-motif formation at an acidic environment.

PAGE analysis revealed that i_2- and i_3-CpG-monomer had significantly higher intermolecular i-motif forming ratio (Figure 11). This result is consistent with the previous study that i-motif DNAs with the sequences such as C_5TC_5 (i_2) and C_6TC_6 (i_3) favor the intermolecular folding of i-motifs.[68,71] The results above showed that i_2- and i_3-CpG-monomers had lower intermolecular i-motif forming ratio than i_1- and i_4-CpG-monomers. To efficiently form i-motif quadruplex, longer sequences of cytosine would be appropriate. However, it is reported that the single-T linker of C_5TC_5 (i_2) and C_6TC_6 (i_3) is not enough to span the groove of the i-motif structure compared to triple-T linker of $C_5T_3C_5$ (i_4).[71] Because i_x-CpG-monomers which I used in this study contain not only i-motif sequence but also other sequences such as CpG motifs, the efficiency of the formation of i-motif could be different from the previous studies.

Agarose gel electrophoretic analysis showed that lssDNA had similar pH-dependent conformational changing properties to those of monomers. I further showed that i_3-CpG-lssDNA formed hydrogel with stronger viscosity at an acidic environment than i_2-CpG-lssDNA. This would be because longer cytosine tracts allowed to form more stable i-motifs. Increasing the length of cytosine tracts was reported to improve the thermal stability of i-motif.[71] Therefore, i_3-CpG-lssDNA with longer cytosine tracts than other lssDNAs used in this study could provide firmer hydrogel.

There exist various types of DNases in blood, tissue, endosome, lysosome, and cytosol.[72–75] Among them, DNase I and DNase II are assumed to be relevant to this study. DNase I is secreted to extracellularly, and DNase II is expressed within endosomes and lysosomes. Once lssDNA is administered intradermally, it is first exposed to the degradation by DNase I. As shown in CHAPTER

1, lssDNA is supposed to be taken up by MSR1 prior to stimulation of TLR9. LssDNA is taken up by macrophages and dendritic cells via MSR1, otherwise it is degraded by DNase I. LssDNA is longer than 10 kb (Figure 12), and it would be taken up efficiently. After the cellular uptake, lssDNA faces degradation by DNase II in endosomes and lysosomes. In this compartment, hydrogelation allowed lssDNA to be more resistant to DNase as follows. DNA hydrogel made of i-motif had low liquidity, and it is suggested that DNase could not access to the core of the DNA hydrogel. The limited DNase II access to lssDNA due to hydrogelation enabled it to be more resistant to degradation, resulting in sustained induction of proinflammatory cytokines *in vitro* and *in vivo*. Therefore, it is assumed that i_3-CpG-lssDNA showed potent and continuous immuno-stimulation through avoiding degradation by DNase I and II in each process.

When lssDNAs were intradermally injected, the expression levels of *Il-6* and *Cxcl9* were likely to be elevated at the injection site. On the other hand, at the lymph nodes, that of *Il-6* was elevated later than at the injection site. Macrophages and dendritic cells at the injection site migrate to lymph nodes. The intracellular degradation of i_3-CpG-lssDNA would be retarded, leading to the obtained results explained above. The expression level of *Cxcl9* was not elevated at the lymph node. IL-6 is secreted not only from macrophages and dendritic cells but also from various cells such as T cells and B cells.[76] Therefore, it is possible that T cells and B cells in the lymph node are activated by dendritic cells and macrophages migrated from injection site of CpG DNAs to express IL-6. On the other hand, CXCL9 is produced only from myeloid cells such as macrophages and dendritic cells.[77] Thus, the result that expression of *Cxcl9* was not elevated in the lymph nodes implies that the administered lssDNAs were hardly transferred to lymph nodes and that the number of dendritic cells and macrophages migrated to lymph node from the injection site was small.

CpG DNA is expected to be used as vaccine adjuvants, cancer immunotherapy, therapeutic medicines for infectious diseases and allergic diseases. PS-modified CpG ODNs are already used in

clinical practice as a vaccine adjuvant for Hepatitis B.[61,78] Clinical trials of concomitant therapies using CpG DNA-containing TLR9 agonist and immune checkpoint inhibitors are underway.[56,79] In addition, development of CpG DNA-based therapies is widely studied.[80,81] i-Motif-containing lssDNA reported here can achieve long-lasting stimulation of TLR9, which might further promote the development of these novel therapies.

In this chapter, I have developed a potent and sustainable immunostimulatory CpG-containing lssDNA utilizing i-motifs. Intermolecular i-motif- and CpG motif-containing lssDNA could serve as a potent and novel nucleic acid therapeutic.

CHAPTER 3

Construction of long single-stranded DNA therapeutics targeting cytosolic DNA sensor proteins

3.1. Introduction

Cytosolic DNA sensor (CDS) is one kind of pattern recognition receptors which senses abnormal DNA existing in the cytosol. Representative CDSs include cGAS (cyclic GMP-AMP synthase),[82] DDX41 (DEAD-Box helicase 41),[83] DAI (DNA-dependent activator of interferon-regulatory factors),[84] AIM2 (absent in melanoma 2), and IFI16 (interferon γ inducible protein 16).[85] CDSs activate STING (stimulator of interferon genes), and induce the expression of type 1 interferon (IFN).[86] This innate immune system protecting from bacterial and viral infections has recently attracted attentions as a target of drug discovery for cancer immunotherapy.[87,88]

Multiple agonists for CDS have been reported.[85,86,89] Most of the reported CDS agonists are double-stranded DNA with various lengths from dozens to thousands base pairs.[85,86,89] CDS activates STING via multiple pathways. A representative and well-studied CDS is cGAS. When cGAS is stimulated by cytosolic DNA, a cyclic dinucleotide, cyclic GMP-AMP (cGAMP) is synthesized from endogenous GTP and ATP existing in the cytosol, which acts as an agonist of STING.[90,91] In addition to cGAMP, various synthetic cyclic dinucleotides have been chemically synthesized and studied so far, aiming for clinical application.[88] Despite these development, these molecules have low membrane permeability, and transfection reagents are required for their efficient delivery to the cytosol.[92,93] Attentions must be paid to systemic toxicities caused by transfection reagents.[94,95] It is desirable to develop delivery strategies to the cytosol free from transfection reagents.

RCA method, used in CHAPTER 2, can enzymatically synthesize lssDNA with periodic sequences. LssDNA produced by RCA reaction has more than 10 kb long, and efficiently taken up by macrophages and dendritic cells. In this study, therefore, I considered facilitation of intracellular transport of lssDNA from endosomes to cytosol using an endosome-disruptive GALA peptide would be a rational design for the development of an effective CDS agonist. GALA peptide is a 30-residue synthetic peptide which includes abundant glutamic acid.[96] Its conformation converts from a random

coil to α-helical structure when the pH is reduced from 7.4 to 5.0. By this conformational change, GALA peptides become more hydrophobic and obtain the ability of destabilizing lipid membranes.

Utilizing this physicochemical property, GALA peptides are used as drug delivery reagents.[97–99] In physiological neutral pH, GALA peptides have negative charges of glutamic acid and more hydrophilic than in acidic environment. It is assumed that GALA peptide is hardly taken up by the cells only by simply mixing lssDNA and GALA peptide. To load GALA peptide to lssDNA, GALA peptide was conjugated to ODNs which can hybridize to lssDNA to obtain peptide-DNA conjugates (PDCs). Figure 16 shows the schematic illustration of PDC used in this study. PDC would enable GALA peptide and lssDNA to be taken up by immune cells simultaneously.

Here, I constructed a novel technology to deliver lssDNA to cytosol, followed by stimulation of CDS. I synthesized the GALA peptide-ODN conjugate, and applied it to a functional nucleic acid therapeutic of CDS agonists. PDC promoted the secretion of IFN-β via CDS from dendritic cells by facilitation of the endosomal escape of lssDNA,

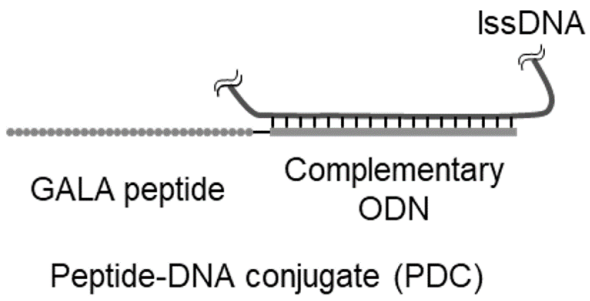

Figure 16. Schematic illustration of the method to load GALA peptide to lssDNA. GALA peptide and oligodeoxynucleotide (ODN) complementary to lssDNA are conjugated (PDC). LssDNA have periodic sequences, and multiple GALA peptides can be loaded to lssDNA by this method.

3.2. Materials & Methods

3.2.1. Chemicals

GALA peptide (NH_2−WEAALAEALAEALAEHLAEALAEALEALAA-COOH) was obtained from GenScript Inc. (Piscataway, NJ). *N*-(4-Maleimidobutyryloxy)succinimide (GMBS) was purchased from Tokyo Chemical Industry Co., Ltd. (Tokyo, Japan). *N*,*N*-Diisopropylethylamine (DIPEA) and *N*,*N*-dimethylformamide (DMF) was obtained from Nacalai Tesque. All other chemicals were of the highest grade available and were used without further purification.

3.2.2. RCA reaction

RCA products (lssDNA) were enzymatically synthesized and obtained as described in CHAPTER 2. Cy5-labeled lssDNA was synthesized by addition of 20 μM Cy5-dCTP (TriLink BioTechnologies, San Diego, CA) to 2 mM dNTPs.

3.2.3. Cells

DC2.4 cells, a murine dendritic cell line, were kindly gifted by Dr. K. L. Rock (University of Massachusetts Medical School), and cultured in Roswell Park Memorial Institute (RPMI) 1640 medium (Nissui Pharmaceutical Co., Ltd.), supplemented with 10% heat-inactivated FBS, 0.2% sodium bicarbonate, 100 IU/mL penicillin, 100 μg/mL streptomycin, 2 mM L-glutamine, 0.5 mM monothioglycerol, and 0.5 mM non-essential amino acids. Cells were cultured at 37 °C in humidified air containing 5% CO_2.

3.2.4. ODNs

Sequences of the ODNs used are shown in Table 5. LssDNA template and primer for lssDNA were obtained from FASMAC Co., Ltd. ODN-A thiol-modified at the 5′-end (SH-ODN-A) was

purchased from Japan Bio Services Co., Ltd.

Table 5. Sequences of the ODNs used in this study.

Name	Sequences (5′ → 3′)
LssDNA template	ACTTGCAGTCTCTAAGGTCAG
(5′-end is phosphate-modified.)	GCATCAGGCATTGAGAAGCTCTC
Primer for lssDNA	GACTGCAAGTGAGAGCTTCT
ODN-A	GAAGCTCTCACTTGCAGT

3.2.5. Ethanol precipitation

Ethanol precipitation was conducted as described in CHAPTER 2 without addition of glycogen to avoid its disturbance to the reaction.

3.2.6. Preparation of GALA peptide-DNA conjugates

Scheme 1 shows the chemical synthesis of GALA peptide-DNA conjugate (PDC). GALA peptide (10 mg/mL in DMF; 1 eq.), GMBS (10 mg/mL in DMF; 1 eq.), and DIPEA (> 1eq.) were mixed at room temperature (22-25 °C) for 24 h. SH-ODN-A was reduced by 0.1 M Tris(2-carboxyethyl)phosphine hydrochloride (TCEP) in water for 1 h at room temperature because some portions of SH-ODN-A formed dimers through the disulfide bond. Reduced SH-ODN-A was purified by ethanol precipitation, and then they were dissolved in PBS (pH 7.4) with 50 mM EDTA to a final concentration of 1 μM. Reduced SH-ODN-A (1 eq.) was added to the reaction mixture of GALA peptide and GMBS, and mixed at room temperature for 24 h. The reaction mixture was subjected to 7 M urea-denaturing 18% PAGE for purification of PDC. Bands corresponding to PDC that were visualized by UV shadowing were excised from the gel, pulverized and extracted with water at 37 °C overnight. PDC was isolated by ethanol precipitation. The product was characterized by matrix-

assisted laser desorption/ionization coupled to time-of-flight mass spectrometry (MALDI-TOF) using AXIMA-CFR Plus (SHIMADZU CORPORATION, Kyoto, Japan) following the previous report.[100] Calculated mass, $[M+2H]^{2+}$ = 4435.18; found mass, $[M+2H]^{2+}$ = 4435.43.

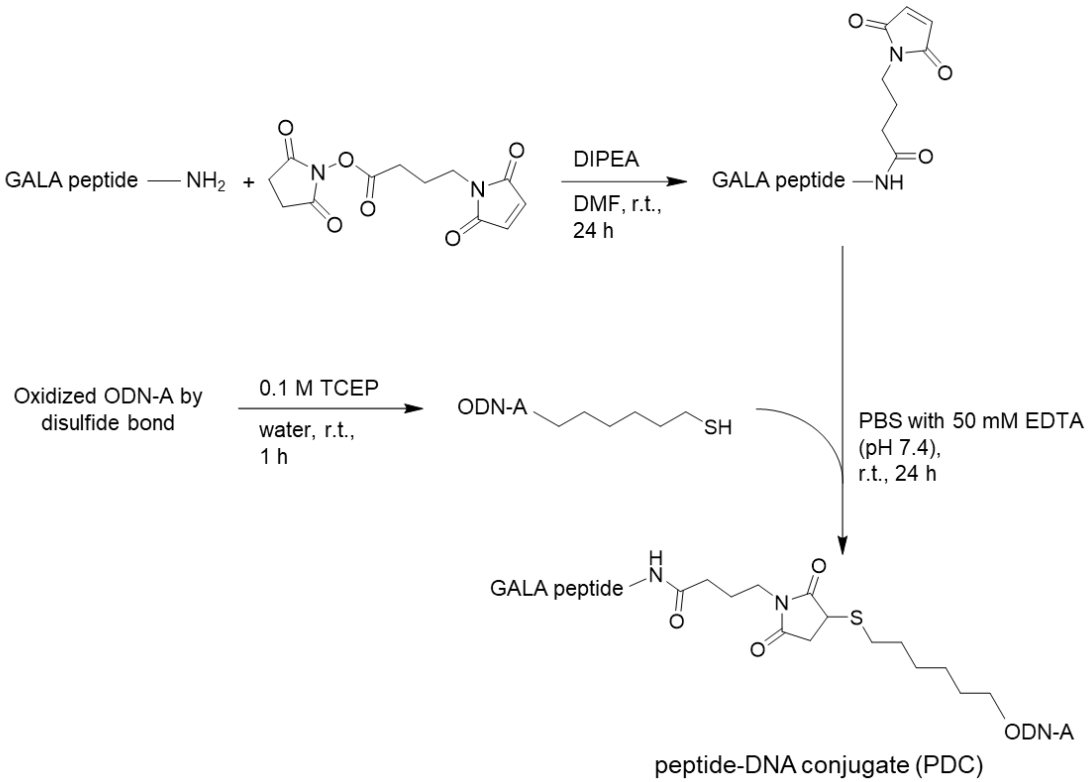

Scheme 1. Synthetic scheme of GALA peptide-DNA conjugate (PDC).

3.2.7. Preparation of calcein-encapsulating liposomes

Calcein-encapsulating liposomes were prepared as follows. First, 41 mg of 1,2-distearoyl-*sn*-glycero-3-phosphocholine (DSPC) and 10 mg of cholesterol were dissolved in chloroform and dried under reduced pressure using a rotary evaporator. The lipid membranes were hydrated in aqueous calcein (60 mM) solution at pH 7.4 in Tris buffer (100 mM). Hydration of lipids was facilitated by shaking for 30 min at 70 °C. Liposomes were extruded through 1 μm pore size polycarbonate membranes using a mini-extruder device (Avanti Polar Lipids, Inc., Birmingham, AL). Sephadex G25

gel filtration was performed to separate unencapsulated calcein from liposomes using citrate buffer (5.9 mM trisodium citrate, 4.5 mM citric acid, 1 mM EDTA-2Na, 100 mM NaCl, pH 5.0) or PBS (pH 7.4). The sizes and ζ potentials of liposomes were measured by Zetasizer Nano ZS (Malvern Instruments, Malvern, UK).

3.2.8. Calcein leakage assay

To evaluate the membrane lytic activity, calcein-encapsulating liposomes (100 μg/mL as a total lipid concentration) were incubated with the indicated concentration of GALA peptide, PDC, or PDC/lssDNA complex. The fluorescent intensities (*FI*) were measured with excitation at 490 nm and emission at 520 nm using Varioskan LUX VLBL00D1 (Thermo Fisher Scientific Inc.). Complete disruption of liposomes was obtained by adding 1% (v/v) Triton X-100 solution. Calcein leakage was calculated as follows:

$$\%\ calcein\ leakage = \frac{FI_{sample} - FI_{buffer}}{FI_{Triton\ X-100} - FI_{buffer}} \times 100$$

3.2.9. Confocal microscopy

DC2.4 cells were seeded on chamber slides at a density of 9 × 10^4 cells/well and then cultured for 24 h. The culture medium was removed, and Cy5-labeled lssDNA (90 μg/mL) or PDC (10 μg/mL as GALA peptide)/Cy5-labeled lssDNA (90 μg/mL) complex was added and cultured for another 6 h. Then, the culture medium was discarded, and incubated with 2.5 μM of LysoTracker Green DND-26 for another 0.5 h. Thereafter, cells were washed twice by PBS, fixed with 4% PFA for 20 min, and washed again twice by PBS. The fixed cells were incubated with 600 nM 4′,6-diamidino-2-phenylindole (DAPI, Life Technologies, Carlsbad, CA) for 5 min at room temperature and washed once. The chamber was then removed and the slide was observed using a confocal microscope (A1R MP, Nikon Instech Co., Ltd., Tokyo, Japan). Twenty cells from the obtained image were randomly

selected, and the shape of each cell was defined as the region of interest (ROI). Colocalization between Cy5 and LysoTracker Green was evaluated by calculating Pearson's correlation coefficient with ImageJ in each ROI.[101]

3.2.10. IFN-β release from DC2.4 cells

DC2.4 cells were seeded on 96-well plates at a density of 5×10^4 cells/well and cultured for 24 h. The cells were then incubated with lssDNA (90 μg/mL), PDC (10 μg/mL as GALA peptide), lipopolysaccharide (100 ng/mL) for 8 h at 37 °C. The levels of IFN-β in the supernatants were determined by ELISA. A rat anti-mouse IFN-β monoclonal capture antibody (code number: 7891) was purchased from YAMASA CORPORATION (Chiba, Japan), and a detection antibody (rabbit anti-mouse IFN-β polyclonal antibody (catalog number: 32400-1, PBL Assay Science, Piscataway, NJ)) was used, followed by HRP-conjugated donkey anti-rabbit IgG antibody (code number: 711-035-152, Jackson ImmunoResearch, West Grove, PA). The concentration was quantified generating standard curves with recombinant mouse IFN-β (catalog number: 12400-1, PBL Assay Science). Optical density was determined using Multiskan FC (Thermo Fisher Scientific Inc.).

3.2.11. Statistical analysis

Differences were statistically evaluated by Student's t-tests for comparisons between two groups. *P* values less than 0.05 were considered statistically significant.

3.3. Results

3.3.1. GALA peptide-DNA conjugate was obtained.

To obtain PDC, GMBS containing both *N*-hydroxysuccinimide (NHS) ester and maleimide groups was used as a linker between the peptide and the ODN. NHS ester easily reacts with primary amine, and maleimide is used to the conjugation with thiol-modified compounds. These reactions provide stable covalent bonds, and thus GMBS has been used as linkers of compounds for biomedical applications.[102,103] Here, to conjugate GALA peptide and ODN-A, N-terminus of GALA peptide was reacted to NHS ester of GMBS. Subsequently, SH-ODN-A was reacted to maleimide of GMBS (Scheme 1). Purified PDC was characterized by MALDI-TOF mass spectrometry and PAGE (Figure 17). An apparent band shift was observed, suggesting the successful conjugation reaction.

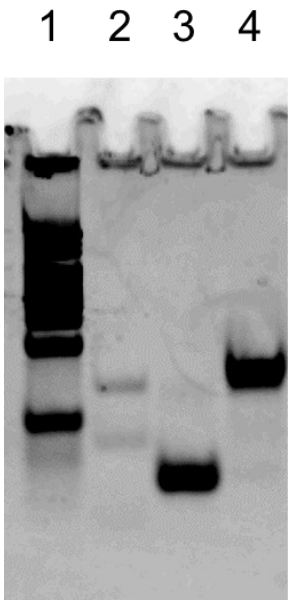

Figure 17. PAGE (18%, 37.5:1 acrylamide/bisacrylamide) analysis of thiol-ODN and purified PDC. The gel was run at room temperature at 250 V for 30 min in 1 ×TBE buffer. The gel was stained by SYBR Gold, and the fluorescence of the gel is shown. Lane 1, 20 bp ladder; lane 2, poly deoxy-thymine with 10, 20, and 30 bases; lane 3, 5′-thiol ODN-A (reduced by TCEP); lane 4, purified PDC.

3.3.2. Hybridizing conditions of lssDNA and its complementary ODNs were optimized.

To load PDC to lssDNA, I investigated the hybridizing conditions of ODN-A and lssDNA. Specifically, I examined two things; 1) molecular ratio of ODN-A and lssDNA and 2) whether or not annealing by heating and gradual cooling is necessary. Figure 18A shows the PAGE analysis of ODN-A and lssDNA varying those conditions. There are no apparent differences between samples with heating and gradual cooling and those with only mixing at room temperature (20 °C), suggesting that it is not necessary to heating and gradual cooling to hybridize ODN-A and lssDNA. In addition, when the molecular ratio of ODN-A to lssDNA was 1:1, the lower band of ODN-A was observed. On the other hand, when the ratio was 1:2, the lower band was almost disappeared, indicating the hybridization of ODN-A and lssDNA. To evaluate the molecular ratio in more detail, 1:1, 1:1.2, 1:1.4, 1:1.6, 1:1.8, and 1:2 were analyzed (Figure 18B). It was revealed that the ratio of 1:2 was most efficient to load ODN-A to lssDNA, and this mixing ratio was used for subsequent experiments.

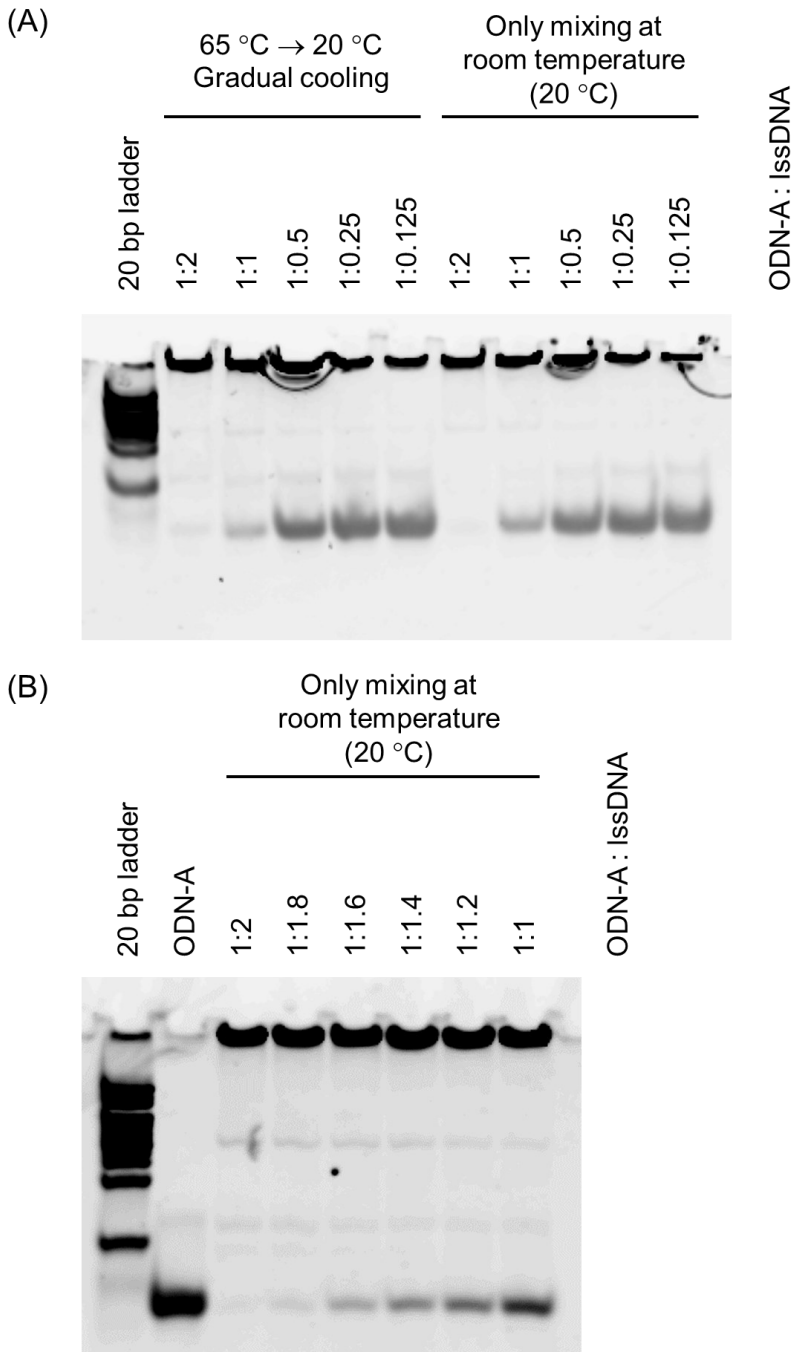

Figure 18. PAGE (18%, 37.5:1 acrylamide/bisacrylamide) analysis of ODN-A and IssDNA. The gel was run at room temperature at 25 V for 30 min, and stained by SYBR Gold. (A) ODN-A and IssDNA were mixed by indicated molecular ratio. Samples with heating and gradual cooling and those only mixing at room temperature were analyzed. (B) ODN-A and IssDNA were mixed at room temperature by indicated molecular ratio.

3.3.3. GALA-DNA conjugate collapsed liposomes under acidic condition.

In acidic conditions in endosome, GALA peptide changes its conformation to exert membrane lytic activity, resulting in endosomal collapse. To evaluate its membrane lytic ability of PDC and PDC/lssDNA complex, calcein-encapsulating liposomes were used. Calcein is a fluorescent dye, and it can be used for evaluation of liposome disruption.[98,104] Calcein self-quenches when encapsulated in liposomes, but the fluorescent intensity increases when liposomes are disrupted and calcein is released. Calcein-encapsulating liposomes were obtained, and their sizes and ζ potentials were measured (Table 6).

Membrane lytic activities of GALA peptide, PDC, and PDC/lssDNA were confirmed using these liposomes (Figure 19). Calcein leakage from liposomes were observed by PDC and PDC/lssDNA complex in addition to GALA peptide in pH-dependent and concentration-dependent manners. This indicates that membrane lytic abilities of GALA peptide were little affected by conjugation reaction and hybridizing to lssDNA.

Table 6. The sizes and ζ potentials of calcein-encapsulating liposomes prepared in pH 5.0 and pH 7.4.

Name	Size (nm)	ζ potential (mV)
Liposomes in pH 5.0	614.3 ± 127.8	-11.1 ± 2.6
Liposomes in pH 7.4	767.7 ± 111.6	-11.3 ± 1.8

Results are expressed as means ± SD (n = 3).

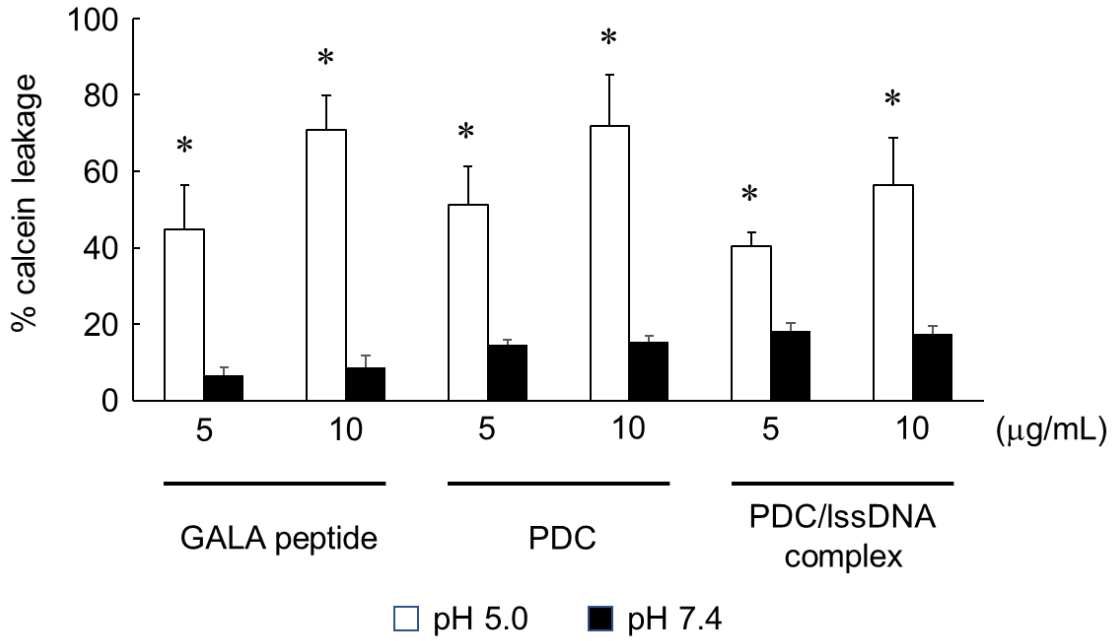

Figure 19. Membrane lytic activities of GALA peptide, PDC, and PDC/lssDNA complex in pH 5.0 and pH 7.4. Calcein-encapsulating liposomes were incubated with the indicated concentration of GALA peptide, PDC, and PDC/lssDNA. Each concentration is standardized with the concentration of GALA peptide. The fluorescent intensities were measured with excitation at 490 nm and emission at 520 nm. Results are shown mean + SD (n = 4). *P < 0.05 compared with % calcein leakage in pH 7.4 at the same concentration.

3.3.4. GALA-DNA conjugate enhanced endosomal escape of lssDNA.

To evaluate the endosomal escape of lssDNA with or without PDC, the intracellular localization of Cy5-labeled lssDNA was observed. The molecular sizes of Cy5-labeled lssDNA and non-labeled lssDNA were confirmed by alkaline agarose gel electrophoresis, which revealed that there were little differences (Figure 20). Murine dendritic cell line DC2.4 cells were added with Cy5-labeled lssDNA or PDC/Cy5-labeled lssDNA complex, and incubated for 6 h. Figure 21A shows the intracellular localization observed by confocal microscopy. Lysosomes and nuclei were fluorescently stained by LysoTracker Green and DAPI, respectively. When DC2.4 cells were incubated with Cy5-lssDNA, lssDNA were well colocalized with lysosomes. On the other hand, when the cells were incubated with PDC/Cy5-labeled lssDNA complex, lssDNA was less colocalized with lysosomes and more distributed to cytosol than when incubated with Cy5-lssDNA only. In addition, the fluorescent intensities of LysoTracker Green and Cy5-labeled lssDNA in PDC/Cy5-labeled lssDNA group were seemed to be weak compared to Cy5-labeled lssDNA group, suggesting that the number of lysosomes were reduced by membrane lytic activity of PDC.

As a quantitative index of colocalization, I analyzed Pearson's correlation coefficient between the red signal (Cy5-labeled lssDNA) and the green signal (LysoTracker Green), and found the PDC/Cy5-labeled lssDNA group significantly had a smaller correlation coefficient than Cy5-labeled lssDNA group (Figure 21B), indicating that lssDNA was less colocalized with lysosomes. These results suggest that endosomal escape of lssDNA was promoted by PDC.

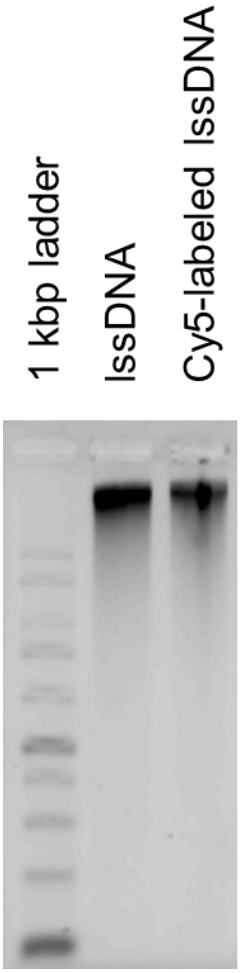

Figure 20. Alkaline agarose gel (1% agarose, 50 mM NaOH, 1 mM EDTA-2Na) electrophoresis of lssDNA and Cy5-labeled lssDNA. The gel was run at 30 V for 6 h at room temperature, and it was stained by SYBR Gold.

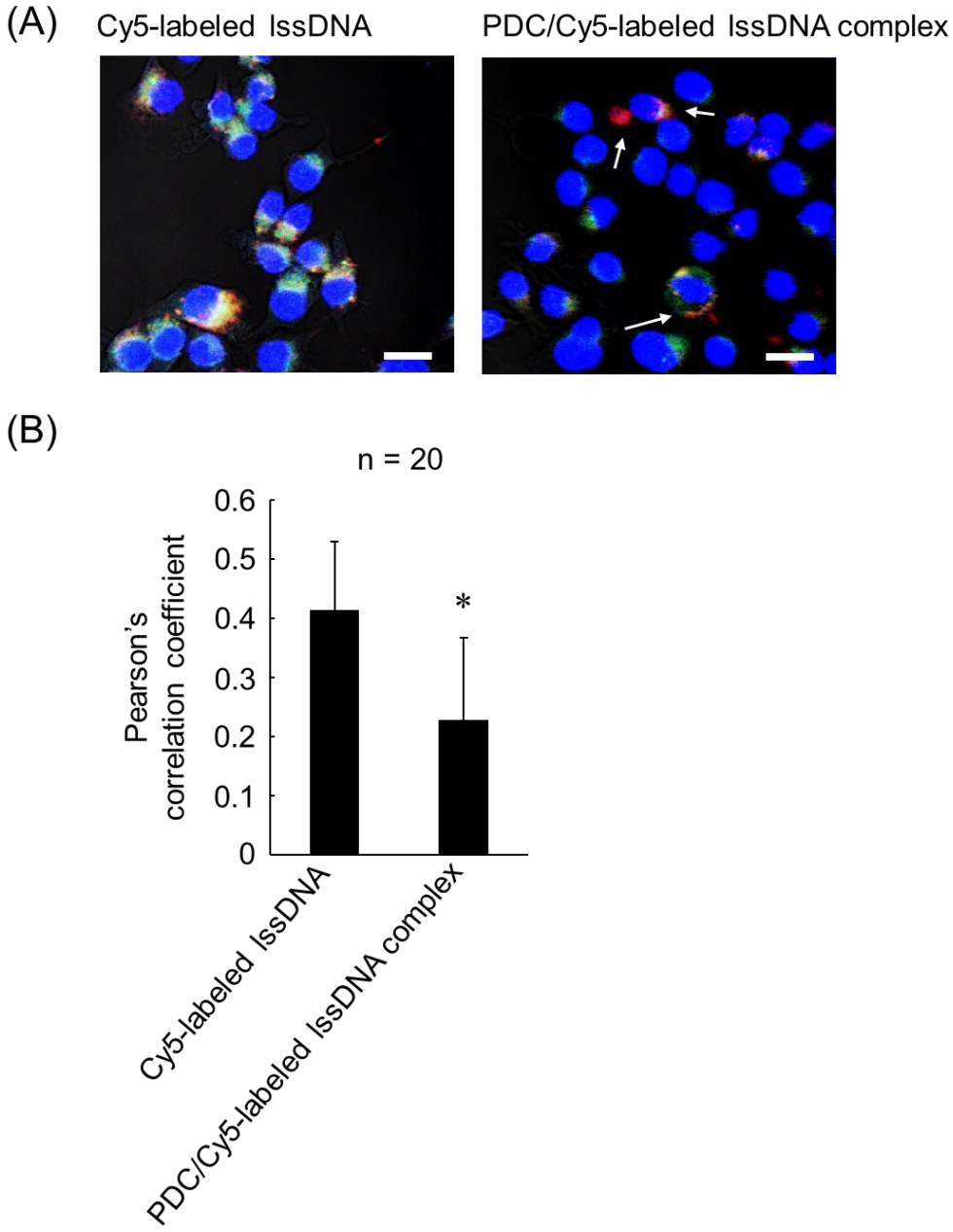

Figure 21. Intracellular localization of Cy5-labeled IssDNA and PDC/Cy5-labeled IssDNA in DC2.4 cells. (A) Confocal microscopic images. DC2.4 cells were incubated with Cy5-labeled IssDNA (90 μg/mL as DNA) and PDC (10 μg/mL as GALA peptide) for 6 h. Lysosomes were stained by LysoTracker Green. White arrows indicate representative cells in which Cy5-labeled IssDNA were delocalized with lysosomes. Scale bar = 50 μm. (B) Pearson's correlation coefficients of representative 20 cells in each image were calculated by ImageJ. The results are expressed as mean + SD (n = 20). *P < 0.05 compared with Cy5-labeled IssDNA.

3.3.5. GALA-DNA conjugate improved secretion of IFN-β from DC2.4 cells.

Stimulation of CDS induces type 1 IFN secretion via STING. To evaluate the agonistic activities of PDC/lssDNA complex, IFN-β secretion from DC2.4 cells were measured by ELISA after incubation with PDC/lssDNA complex for 8 h, compared with lssDNA and the mixture of GALA peptide and lssDNA (GALA/lssDNA) (Figure 22A). Constant secretion of small amounts of IFN-β from DC2.4 cells was observed, and the secretion of IFN-β increased when lssDNA and GALA/lssDNA were added. However, secretion of IFN-β significantly increased when PDC/lssDNA complex was added, compared to lssDNA and GALA/lssDNA. These results suggest that GALA peptide was more taken up by cells when GALA peptide was used as PDC, which can easily load to lssDNA.

To prove that IFN-β was secreted through the designed pathway of endosomal escape of lssDNA by GALA peptide followed by CDS stimulation, I used chloroquine and RU.521 as inhibitors. Chloroquine inhibits endosomal acidification, resulting in attenuation of the membrane lytic effect of GALA peptide in endosomes.[98] RU.521 is an inhibitor of cGAS, that is one of the CDSs.[105] Figure 22B shows IFN-β release from DC2.4 cells when added with 5 μM chloroquine or 0.1 μg/mL RU.521. Chloroquine inhibited IFN-β release in GALA/lssDNA and PDC/lssDNA complex samples. This indicates that the membrane lytic PDC activity was inhibited although small amounts of GALA peptide was also taken up to promote endosomal escape. Moreover, RU.521 inhibited IFN-β release of every sample to almost the same level, suggesting that most of the IFN-β release was mediated by cGAS. I confirmed that IFN-β release was hardly affected by these inhibitors when the cells were stimulated by a TLR4 agonist lipopolysaccharide (100 ng/mL), an independent pathway of CDS-STING pathway (Figure 22B).

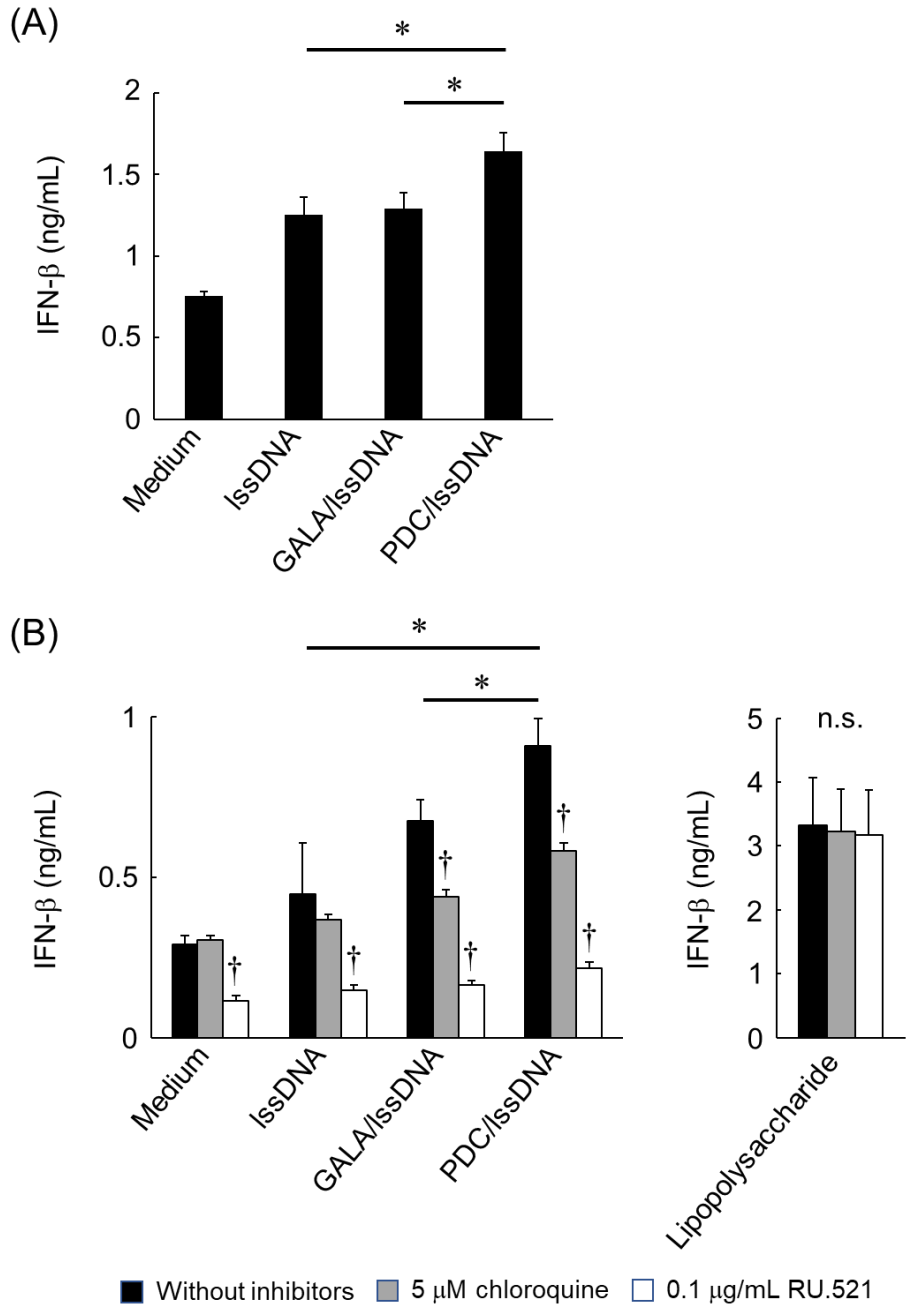

Figure 22. IFN-β release from DC2.4 cells. (A) DC2.4 cells were incubated with lssDNA (90 μg/mL), GALA peptide (10 μg/mL), and PDC (10 μg/mL as GALA peptide) for 8 h. Results are expressed as mean + SD (n = 4). **P* < 0.05. (B) DC2.4 cells were incubated with or without inhibitors. Lipopolysaccharide (100 ng/mL) was used as a positive control with CDS-STING independent pathways. Results are expressed as mean + SD (n = 4). * *P* < 0.05, † *P* < 0.05 compared with "without inhibitors" samples.

3.4. Discussion

In this chapter, I synthesized GALA-peptide-DNA conjugate (PDC), and constructed functional nucleic acid by hybridizing PDC to lssDNA which stimulates CDS. CDS-STING pathway has been attracted as a therapeutic target of cancer immunotherapy because of secretion of type 1 IFN. Stimulation of STING and production of type 1 IFN activate natural killer cells (NK cells),[106] induce costimulatory factors of dendritic cells,[107,108] and enhance T cell infiltration.[109] CDS agonists would be useful for cancer immunotherapy by these immunomodulatory pathways.

Peptide-DNA conjugates and its application to biomedical and pharmaceutical field have been widely studied.[110–112] In these studies, peptide conjugation methods were aimed at the delivery of antisense oligonucleotides to a specific cell. In this study, peptide conjugation was used to facilitate the endosomal escape of lssDNA. Peptides have various functions due to the diversity of amino acids, and therefore, peptide conjugation with DNA would promote the therapeutic application of nucleic acids.

Confocal microscopic images showed GALA-peptide conjugated DNA successfully enhanced the endosomal escape of lssDNA (Figure 21). LssDNA had more than 10 kb length (Figure 20) and the density of negative charges are estimated to be higher than those of ODNs. As shown in CHAPTER 1, negatively-charged DNA is taken up via MSR1 to endosomes and lysosomes. Colocalization of Cy5-labeled lssDNA and LysoTracker Green explains this transport of lssDNA to endosomes and lysosomes. On the other hand, the reduced signal of LysoTracker Green in PDC/lssDNA complex group implies that endosomes and lysosomes were collapsed due to the membrane lytic activity of PDC. Also, Cy5-labeled lssDNA which escaped from endosomes was diluted in the cytosol, resulting in weaker signals of Cy5 in PDC/Cy5-labeled lssDNA than in Cy5-labeled lssDNA.

In Figure 22, PDC/lssDNA significantly increased IFN-β release compared to GALA/lssDNA. GALA peptide is rich in glutamic acid, making it anionic in neutral pH conditions. This would cause an electrostatic repulsion between GALA peptide and lssDNA, and GALA peptide was not taken up by the cells so much. Thus, conjugation of GALA peptide and ODN was necessary. Decreases of IFN-β release by chloroquine proved that GALA peptide exerted its membrane lytic activity within endosomes. Moreover, inhibition by RU.521 proved that the IFN-β release was mediated by cGAS-STING pathway. DC2.4 cells produced a small amount of IFN-β without any compounds, which was inhibited by RU.521. This result implied that DC2.4 cells produced IFN-β through cGAS-STING pathway even under normal conditions.

Cancer immunotherapy modulates the immune system in tumor microenvironment (TME). The target of CDS agonists are macrophages and dendritic cells in TME. As discussed above, lssDNA is efficiently delivered to macrophages and dendritic cells without any chemical modifications and any transfection reagents. This could be the advantage compared with other CDS agonists and cyclic dinucleotides (STING agonists), which have low membrane permeability.

In this chapter, I constructed the functional lssDNA that targets cytosolic DNA sensors through conjugation to GALA peptide. This novel type of CDS agonists would be useful and applicable for cancer immunotherapy.

CONCLUSION

Recently, nucleic acid therapeutics have attracted attentions, and they are widely studied and beginning to be used in clinical practice. Development of suitable delivery systems accelerates those researches. In this thesis, to provide long single-stranded DNA (lssDNA) with functions as novel therapeutics by the control of intracellular distribution, I designed three chapters.

In CHAPTER 1, I aimed to elucidate the cellular uptake mechanism of DNA prior to the development of lssDNA therapeutics. Previous studies of our group showed DNA nanostructures with higher densities of negative charges are efficiently taken up by immune cells. Also, polypod-like nanostructured DNA (polypodna) are taken up by macrophage scavenger receptor 1 (MSR1). However, the responsible receptors for DNA uptake and their contributions were yet to be elucidated. The obtained results consistently showed that MSR1 plays a central role in DNA uptake through efficient interaction of MSR1 and DNA with high negative-charge density. This implies long single-stranded DNA (lssDNA) synthesized by rolling circle amplification (RCA) reaction would be efficiently delivered to the endosomes of MSR1-expressing immune cells (macrophages and dendritic cells), leading to the use of lssDNA for the subsequent studies.

In CHAPTER 2, I attempted to develop lssDNA with long-lasting endosome-targeting ability. Unmethylated CpG motifs are recognized by Toll-like receptor 9 (TLR9), which is expressed in endosomes of immune cells, leading to secretion of proinflammatory cytokines. CpG DNA is, therefore, expected to be used for the treatment of cancers, infectious diseases, and allergic diseases. Incorporation of CpG motifs into lssDNA would efficiently deliver them to TLR9 due to the results obtained in CHAPTER 1. Moreover, to retain lssDNA within endosomes for longer period of time, I introduced i-motif sequences to CpG-containing lssDNA. i-Motif and CpG- incorporated lssDNA formed hydrogel in acidic condition like in endosome, and it induced long-lasting and potent cytokine

release both *in vitro* and *in vivo*, suggesting that it could serve as a novel therapeutic TLR9 agonist with long-lasting stimulation properties.

In CHAPTER 3, I designed and constructed cytosol-targeting lssDNA. Cytosolic DNA sensor (CDS) proteins sense DNA in the cytosol, leading to the activation of stimulator of interferon genes (STING) and production of type 1 interferon (IFN). Thus, it is expected as the target of vaccine adjuvant and cancer immunotherapy. I considered lssDNA as an efficient agonist of CDS, and GALA peptide, an endosome-disruptive peptide was used to deliver lssDNA to cytosol. GALA peptide and oligonucleotide complementary to lssDNA are conjugated, and peptide-DNA conjugates (PDCs) were successfully obtained. By hybridizing PDC to complementary lssDNA (PDC/lssDNA), endosomal escape of lssDNA was promoted and induced more amount of IFN-β, indicating efficient stimulation of CDS-STING pathway. GALA peptide-conjugated DNA would be a helpful pharmaceutical tool to develop cytosol delivery systems of nucleic acids.

The obtained findings in this thesis will lead to the development of more effective nucleic acid therapeutics, and will widen them to clinical applications.

LIST OF PUBLICATIONS INCLUDED IN THIS THESIS

Critical contribution of macrophage scavenger receptor 1 to the uptake of nanostructured DNA by immune cells.

Umemura K, Ohtsuki S, Nagaoka M, Kusamori K, Inoue T, Takahashi Y, Takakura Y, Nishikawa M. ***Nanomedicine***. 2021;34:102386.

Development of unmethylated CpG DNA with long-lasting endosome-targeting ability by i-motifs.

Oda W, **Umemura K**, Ito K, Kawamoto Y, Takahashi Y, Takakura Y.

Manuscript in preparation

Activation of cytosolic DNA sensor-STING pathway by GALA peptide-loaded long single-stranded DNA.

Umemura K, Kawamoto Y, Takahashi Y, Takakura Y.

Manuscript in preparation

OTHER PUBLICATIONS

Combined use of chemically modified nucleobases and nanostructured DNA for enhanced immunostimulatory activity of CpG oligodeoxynucleotide.

Araie Y, Ohtsuki S, Park S, Nagaoka M, **Umemura K**, Sugiyama H, Kusamori K, Takahashi Y, Takakura Y, Nishikawa M. ***Bioorg Med Chem***. 2021;29:115864.

ACKNOWLEDGMENT

First and foremost, I would like to express my deepest gratitude to Professor Yoshinobu Takakura, PhD, from the Department of Biopharmaceutics and Drug Metabolism, Graduate School of Pharmaceutical Sciences, Kyoto University, for his patient, consistent, and critical guidance and warm encouragement through seven years, which enabled me to complete my PhD course. He has always guided me in the right direction.

Then, I would like to express my sincere gratitude to Professor Makiya Nishikawa, PhD, from the Laboratory of Biopharmaceutics, Faculty of Pharmaceutical Sciences, Tokyo University of Science, for his insightful and critical advices. I would not have been able to make progress and complete my PhD course without him. I would like to express my respect and admiration to him for his attitude to and enthusiasm for research.

As my direct supervisor, I would like to express my greatest thanks to Associate Professor Yuki Takahashi, PhD, from the Department of Biopharmaceutics and Drug Metabolism, for his patient and critical advices and assistances. Dr. Takahashi's instructions taught me how to design and conduct independent research and how to solve facing difficulties.

I would like to extend my sincere thanks to Assistant Professor Yusuke Kawamoto, PhD, from the Department of Biopharmaceutics and Drug Metabolism, for his valuable discussion and warm support.

I would like to express gratitude to Professor Kazuo Matsubara, PhD, Professor Tomohiro Terada, PhD, and Associate Professor Atsushi Yonezawa, PhD, from the Department of Clinical Pharmacology and Therapeutics, Graduate School of Pharmaceutical Sciences, Kyoto University, for their kind understandings and supports to my dual career of graduate student and clinical pharmacist. Also, I would like to thank all other colleagues at Kyoto University Hospital.

I would like to thank all the members at the Department of Biopharmaceutics and Drug Metabolism, both the alumni and the current members, for their help with research as well as fantastic memories we have had over the past seven years. I would like to give my special thanks to Ms. Noriko Hikihara, Dr. Shozo Ohtsuki, Dr. Fusae Komura, Dr. Mengmeng Tan, Dr. Koichi Ito, Ms. Wakana Oda, Ms. Natsune Ishikawa, Dr. Wen Liu, Mr. Reiichi Ariizumi, Mr. Shunsuke Nishimura, Mr. Tatsuoki Maezawa, Mr. Yuta Arima, and Dr. Misako Takenaka for their stinting help.

Last but not least, I would like to express my gratitude to my family for raising and educating me. Thank you very much for providing me such a precious opportunity of PhD course and always supporting me.

REFERENCES

1. Anselmo AC, Mitragotri S. An overview of clinical and commercial impact of drug delivery systems. *J Control Release*. 2014;190:15-28.
2. Liu D, Yang F, Xiong F, Gu N. The smart drug delivery system and its clinical potential. *Theranostics*. 2016;6(9):1306-1323.
3. Adepu S, Ramakrishna S, Costa-Pinto R, Oliveira AL. Controlled Drug Delivery Systems: Current Status and Future Directions. *Molecules*. 2021;26(19):5905.
4. Riley RS, June CH, Langer R, Mitchell MJ. Delivery technologies for cancer immunotherapy. *Nat Rev Drug Discov*. 2019;18(3):175-196.
5. Almeida B, Nag OK, Rogers KE, Delehanty JB, Trabocchi A, Lenci E. Recent Progress in Bioconjugation Strategies for Liposome-Mediated Drug Delivery. *Molecules*. 2020;25(23):5672.
6. Liu J, Pandya P, Afshar S. Therapeutic advances in oncology. *Int J Mol Sci*. 2021;22(4):1-41.
7. Vargason AM, Anselmo AC, Mitragotri S. The evolution of commercial drug delivery technologies. *Nat Biomed Eng*. 2021;5(9):951-967.
8. Juliano RL. The delivery of therapeutic oligonucleotides. *Nucleic Acids Res*. 2016;44(14):6518-6548.
9. Gupta A, Andresen JL, Manan RS, Langer R. Nucleic acid delivery for therapeutic applications. *Adv Drug Deliv Rev*. 2021;178:113834.
10. Paunovska K, Loughrey D, Dahlman JE, Coulter WH. Drug delivery systems for RNA therapeutics. *Nat Rev Genet*. 2022;23(5):265-280.
11. Azad RF, Brown-Driver V, Buckheit RW, Anderson KP. Antiviral activity of a phosphorothioate oligonucleotide complementary to human cytomegalovirus RNA when used in combination with antiviral nucleoside analogs. *Antiviral Res*. 1995;28(2):101-111.
12. Gragoudas ES, Adamis AP, Cunningham ET, Feinsod M, Guyer DR. Pegaptanib for neovascular age-related macular degeneration. *N Engl J Med*. 2004;351(27):2805-16.
13. Kastelein JJP, Wedel MK, Baker BF, et al. Potent Reduction of Apolipoprotein B and Low-Density Lipoprotein Cholesterol by Short-Term Administration of an Antisense Inhibitor of Apolipoprotein B. *Circulation*. 2006;114(16):1729-35.
14. Nelson SF, Crosbie RH, Miceli MC, Spencer MJ. Emerging genetic therapies to treat Duchenne muscular dystrophy. *Curr Opin Neurol*. 2009;22(5):532-538.
15. Crooke ST, Geary RS. Clinical pharmacological properties of mipomersen (Kynamro), a second generation antisense inhibitor of apolipoprotein B Keywords antisense inhibitor, familial hypercholesterolaemia, LDL-cholesterol, mipomersen. *Br J Clin Pharmacol*. 2013;76(2):269-76.
16. Corey DR. Nusinersen, an antisense oligonucleotide drug for spinal muscular atrophy. *Nat Neurosci*. 2017;20(4):497-499.

17. Jackson S, Lentino J, Kopp J, et al. Immunogenicity of a two-dose investigational hepatitis B vaccine, HBsAg-1018, using a toll-like receptor 9 agonist adjuvant compared with a licensed hepatitis B vaccine in adults. *Vaccine*. 2018;36(5):668-674.
18. Adams D, Gonzalez-Duarte A, O'Riordan, et al. Patisiran, an RNAi Therapeutic, for Hereditary Transthyretin Amyloidosis. *N Engl J Med*. 2018;379(1):11-21.
19. Nasir Majeed C, Ma CD, Xiao T, Rudnick S, Bonkovsky HL. Spotlight on Givosiran as a Treatment Option for Adults with Acute Hepatic Porphyria: Design, Development, and Place in Therapy. *Drug Des Devel Ther*. 2022;16:1827-1845.
20. Teijaro JR, Farber DL. COVID-19 vaccines: modes of immune activation and future challenges. *Nat Rev Immunol*. 2021;21(4):195-197.
21. Yata T, Takahashi Y, Tan M, et al. Efficient amplification of self-gelling polypod-like structured DNA by rolling circle amplification and enzymatic digestion. *Sci Rep*. 2015;5:14979.
22. Ito K, Kariya M, Yasui K, Takahashi Y, Takakura Y. Development of Hydrophobic Interaction-based DNA Supramolecules as Efficient Delivery Carriers of CpG DNA to Immune cells. *J Pharm Sci*. 2022;111(4):1133-1141.
23. Desmet CJ, Ishii KJ. Nucleic acid sensing at the interface between innate and adaptive immunity in vaccination. *Nat Rev Immunol*. 2012;12(7):479-491.
24. Jorritsma SHT, Gowans EJ, Grubor-Bauk B, Wijesundara DK. Delivery methods to increase cellular uptake and immunogenicity of DNA vaccines. *Vaccine*. 2016;34(46):5488-5494.
25. Watson JD, Crick FHC. Molecular Structure of Nucleic Acids: A Structure for Deoxyribose Nucleic Acid. *Nature*. 1953;171(4356):737-738.
26. Fu Y, Wang X, Zhang J, Li W. Nanomaterials and nanoclusters based on DNA modulation. *Curr Opin Biotechnol*. 2014;28:33-38.
27. Linko V, Dietz H. The enabled state of DNA nanotechnology. *Curr Opin Biotechnol*. 2013;24(4):555-561.
28. Seeman NC. Nucleic acid junctions and lattices. *J Theor Biol*. 1982;99(2):237-247.
29. Rothemund PWK. Folding DNA to create nanoscale shapes and patterns. *Nature*. 2006;440(7082):297-302.
30. Chhabra R, Sharma J, Liu Y, Rinker S, Yan H. DNA Self-assembly for Nanomedicine. *Adv Drug Deliv Rev*. 2010;62(6):617-625.
31. Linko V, Ora A, Kostiainen MA. DNA Nanostructures as Smart Drug-Delivery Vehicles and Molecular Devices. *Trends Biotechnol*. 2015;33(10):586-594.
32. Mohri K, Nishikawa M, Takahashi N, et al. Design and development of nanosized DNA assemblies in polypod-like structures as efficient vehicles for immunostimulatory CpG motifs to immune cells. *ACS Nano*. 2012;6(7):5931-5940.
33. Uno S, Nishikawa M, Mohri K, et al. Efficient delivery of immunostimulatory DNA to mouse and

human immune cells through the construction of polypod-like structured DNA. *Nanomedicine*. 2014;10(4):765-774.

34. Mohri K, Nagata K, Ohtsuki S, et al. Elucidation of the Mechanism of Increased Activity of Immunostimulatory DNA by the Formation of Polypod-like Structure. *Pharm Res*. 2017;34(11):2362-2370.
35. Maezawa T, Ohtsuki S, Hidaka K, et al. DNA density-dependent uptake of DNA origami-based two-or three-dimensional nanostructures by immune cells. *Nanoscale*. 2020;12:14818.
36. Kimura Y, Sonehara K, Kuramoto E, et al. Binding of oligoguanylate to scavenger receptors is required for oligonucleotides to augment NK cell activity and induce IFN. *J Biochem*. 1994;116(5):991-994.
37. Benimetskaya L, Loike JD, Khaled Z, et al. Mac-1 (CD11b/CD18) is an oligodeoxynucleotide-binding protein. *Nat Med*. 1997;3(4):414-420.
38. Sirois CM, Jin T, Miller AL, et al. RAGE is a nucleic acid receptor that promotes inflammatory responses to DNA. *J Exp Med*. 2014;211(5):1001-1001.
39. Siess DC, Vedder CT, Merkens LS, et al. A human gene coding for a membrane-associated nucleic acid-binding protein. *J Biol Chem*. 2000;275(43):33655-33662.
40. Caminschi I, Meuter S, Heath WR. DEC-205 is a cell surface receptor for CpG oligonucleotides. *Oncoimmunology*. 2013;2(3).
41. Moseman AP, Moseman EA, Schworer S, et al. Mannose Receptor 1 Mediates Cellular Uptake and Endosomal Delivery of CpG-Motif Containing Oligodeoxynucleotides. *J Immunol*. 2013;191(11):5615-5624.
42. Brown DA, Kang SH, Gryaznov SM, et al. Effect of phosphorothioate modification of oligodeoxynucleotides on specific protein binding. *J Biol Chem*. 1994;269(43):26801-26805.
43. Watanabe TA, Geary RS, Levin AA. Plasma Protein Binding of an Antisense Oligonucleotide Targeting Human ICAM-1 (ISIS 2302). *Oligonucleotides*. 2006;16(2):169-180.
44. Ohtsuki S, Takahashi Y, Inoue T, Takakura Y, Nishikawa M. Reconstruction of Toll-like receptor 9-mediated responses in HEK-Blue hTLR9 cells by transfection of human macrophage scavenger receptor 1 gene. *Sci Rep*. 2017;7(1):1-9.
45. Sunagawa GA, Sumiyama K, Ukai-Tadenuma M, et al. Mammalian Reverse Genetics without Crossing Reveals Nr3a as a Short-Sleeper Gene. *Cell Rep*. 2016;14(3):662-677.
46. Latz E, Schoenemeyer A, Visintin A, et al. TLR9 signals after translocating from the ER to CpG DNA in the lysosome. *Nat Immunol*. 2004;5(2):190-198.
47. Canton J, Neculai D, Grinstein S. Scavenger receptors in homeostasis and immunity. *Nat Rev Immunol*. 2013;13(9):621-634.
48. Takeuchi O, Akira S. Pattern Recognition Receptors and Inflammation. *Cell*. 2010;140(6):805-820.
49. Doi T, Higashino KI, Kurihara Y, et al. Charged collagen structure mediates the recognition of

negatively charged macromolecules by macrophage scavenger receptors. *J Biol Chem*. 1993;268(3):2126-2133.

50. Baid K, Nellimarla S, Huynh A, et al. Direct binding and internalization of diverse extracellular nucleic acid species through the collagenous domain of class A scavenger receptors. *Immunol Cell Biol*. 2018;96(9):922-934.
51. Matsumoto A, Naito M, Itakura H, et al. Human Macrophage Scavenger Receptors: Primary Structure, Expression, and Localization in Atherosclerotic Lesions. *Proc Natl Acad Sci U S A*. 1990;87(23):9133-7.
52. Gough PJ, Greaves DR, Gordon S. A naturally occurring isoform of the human macrophage scavenger receptor (SR-A) gene generated by alternative splicing blocks modified LDL uptake. *J Lipid Res*. 1998;39(3):531-543.
53. Aguilar JC, Rodríguez EG. Vaccine adjuvants revisited. *Vaccine*. 2007;25(19):3752-3762.
54. Zhu G, Liu Y, Yang X, et al. DNA-inorganic hybrid nanovaccine for cancer immunotherapy. *Nanoscale*. 2016;8:6684.
55. Chen W, Jiang M, Yu W, et al. CpG-Based Nanovaccines for Cancer Immunotherapy. *Int J Nanomedicine*. 2021;16:5281-5299.
56. Ribas A, Medina T, Kirkwood JM, et al. Overcoming PD-1 Blockade Resistance with CpG-A Toll-Like Receptor 9 Agonist Vidutolimod in Patients with Metastatic Melanoma. *Cancer Discov*. 2021;11(12):2998-3007.
57. Zhang L, Zhu G, Mei L, et al. Self-Assembled DNA Immunonanoflowers as Multivalent CpG Nanoagents. *ACS Appl Mater Interfaces*. 2015;7(43):24069-74.
58. Roberto Mineo J, Vilanova M, Lang R, et al. CpG Oligodeoxynucleotides Induce Differential Cytokine and Chemokine Gene Expression Profiles in Dapulian and Landrace Pigs. *Front Microbiol*. 2016;7.
59. Bode C, Zhao G, Steinhagen F, Kinjo T, Klinman DM. CpG DNA as a vaccine adjuvant. *Expert Rev Vaccines*. 2011;10(4):499-511.
60. Nishikawa M, Ogawa K, Umeki Y, et al. Injectable, self-gelling, biodegradable, and immunomodulatory DNA hydrogel for antigen delivery. *J Control Release*. 2014;180(1):25-32.
61. Jackson S, Lentino J, Kopp J, et al. Immunogenicity of a two-dose investigational hepatitis B vaccine, HBsAg-1018, using a toll-like receptor 9 agonist adjuvant compared with a licensed hepatitis B vaccine in adults. *Vaccine*. 2018;36(5):668-674.
62. Zhang H, Chen W, Gong K, Chen J. Nanoscale Zeolitic Imidazolate Framework-8 as Efficient Vehicles for Enhanced Delivery of CpG Oligodeoxynucleotides. *ACS Appl Mater Interfaces*. 2017;9(37):31519-31525.
63. Wei H, Zhao Z, Wang Y, Zou J, Lin Q, Duan Y. One-Step Self-Assembly of Multifunctional DNA Nanohydrogels: An Enhanced and Harmless Strategy for Guiding Combined Antitumor Therapy.

ACS Appl Mater Interfaces. 2019;11(50):46479-46489.

64. Ouyang X, Li J, Liu H, et al. Rolling Circle Amplification-Based DNA Origami Nanostructrures for Intracellular Delivery of Immunostimulatory Drugs. *Small*. 2013;9(18):3082-3087.
65. Ouyang X, Li J, Liu H, et al. Self-assembly of DNA-based drug delivery nanocarriers with rolling circle amplification. *Methods*. 2014;67(2):198-204.
66. Dembska A, Bielecka P, Juskowiak B. pH-Sensing fluorescence oligonucleotide probes based on an i-motif scaffold: a review. *Analytical Methods*. 2017;9(43):6092-6106.
67. Dong Y, Yang Z, Liu D. DNA Nanotechnology Based on i-Motif Structures. *Acc Chem Res*. 2014;47(6):1853-1860.
68. Xu W, Huang Y, Zhao H, et al. DNA Hydrogel with Tunable pH-Responsive Properties Produced by Rolling Circle Amplification. *Chemistry*. 2017;23(72):18276-18281.
69. Padilla-Parra S, Matos PM, Kondo N, Marin M, Santos NC, Melikyan GB. Quantitative imaging of endosome acidification and single retrovirus fusion with distinct pools of early endosomes. *Proc Natl Acad Sci U S A*. 2012;109(43):17627-17632.
70. Smith SA, Selby LI, Johnston APR, Such GK. The Endosomal Escape of Nanoparticles: Toward More Efficient Cellular Delivery. *Bioconjug Chem*. 2019;30(2):263-272.
71. Li T, Famulok M. I-Motif-Programmed Functionalization of DNA Nanocircles. *J Am Chem Soc*. 2013;135(4):1593-1599.
72. Han DSC, Ni M, Chan RWY, et al. The Biology of Cell-free DNA Fragmentation and the Roles of DNASE1, DNASE1L3, and DFFB. *Am J Hum Genet*. 2020;106(2):202-214.
73. Chan MP, Onji M, Fukui R, et al. ARTICLE DNase II-dependent DNA digestion is required for DNA sensing by TLR9. *Nat Commun*. 2015;6:5853.
74. Lo YMD, Han DSC, Jiang P, Chiu RWK. Epigenetics, fragmentomics, and topology of cell-free DNA in liquid biopsies. *Science*. 2021;372(6538).
75. Lauková L, Konečná B, Janovičová ubica, Vlková B, Celec P. Deoxyribonucleases and Their Applications in Biomedicine. *Biomolecules*. 2020;10(7):1036.
76. Xu Y, Cheng M, Shang P, Yang Y. Role of IL-6 in dendritic cell functions. *J Leukoc Biol*. 2022;111(3):695-709.
77. Marcovecchio PM, Thomas G, Salek-Ardakani S. CXCL9-expressing tumor-associated macrophages: new players in the fight against cancer. *J Immunother Cancer*. 2021;9(2):e002045.
78. Eng NF, Bhardwaj N, Mulligan R, Diaz-Mitoma F. The potential of 1018 ISS adjuvant in hepatitis B vaccines: HEPLISAV" review. *Hum Vaccin Immunother*. 2013;9(8):1661-1672.
79. Garon EB, Spira AI, Johnson M, et al. A Phase Ib Open-Label, Multicenter Study of Inhaled DV281, a TLR9 Agonist, in Combination with Nivolumab in Patients with Advanced or Metastatic Non–small Cell Lung Cancer. *Clin Cancer Res*. 2021;27(16):4566-4573.
80. Jain VV, Kitagaki K, Kline JN. CpG DNA and immunotherapy of allergic airway diseases. *Clin*

Exp Allergy. 2003;33(10):1330-1335.

81. Liu W, Ota M, Tabushi M, Takahashi Y, Takakura Y. Development of allergic rhinitis immunotherapy using antigen-loaded small extracellular vesicles. *J Control Release*. 2022;345:433-442.
82. Sun L, Wu J, Du F, Chen X, Chen ZJ. Cyclic GMP-AMP Synthase Is a Cytosolic DNA Sensor That Activates the Type I Interferon Pathway. *Science*. 2013;339(6121):786-791.
83. Zhang Z, Yuan B, Bao M, Lu N, Kim T, Liu YJ. The helicase DDX41 senses intracellular DNA mediated by the adaptor STING in dendritic cells. *Nat Immunol*. 2011;12(10):959-965.
84. Takaoka A, Wang Z, Choi MK, et al. DAI (DLM-1/ZBP1) is a cytosolic DNA sensor and an activator of innate immune response. *Nature*. 2007;448(7152):501-505.
85. Unterholzner L, Keating SE, Baran M, et al. IFI16 is an innate immune sensor for intracellular DNA. *Nat Immunol*. 2010;11(11):997-1004.
86. Unterholzner L. The interferon response to intracellular DNA: Why so many receptors? *Immunobiology*. 2013;218(11):1312-1321.
87. Jiang M, Jiang M, Chen P, et al. cGAS-STING, an important pathway in cancer immunotherapy. *J Hematol Oncol*. 2020;13(1).
88. Amouzegar A, Chelvanambi M, Filderman JN, Storkus WJ, Luke JJ. STING agonists as cancer therapeutics. *Cancers (Basel)*. 2021;13(11).
89. Zahid A, Ismail H, Li B, Jin T. Molecular and Structural Basis of DNA Sensors in Antiviral Innate Immunity. *Front Immunol*. 2020;11:613039.
90. Hopfner KP, Hornung V. Molecular mechanisms and cellular functions of cGAS–STING signalling. *Nat Rev Mol Cell Biol*. 2020;21(9):501-521.
91. Ablasser A, Goldeck M, Cavlar T, et al. cGAS produces a 2′-5′-linked cyclic dinucleotide second messenger that activates STING. *Nature*. 2013;498(7454):380-384.
92. Yildiz S, Alpdundar E, Gungor B, et al. Enhanced immunostimulatory activity of cyclic dinucleotides on mouse cells when complexed with a cell-penetrating peptide or combined with CpG. *Eur J Immunol*. 2015;45(4):1170-1179.
93. Gogoi H, Mansouri S, Jin L. The Age of Cyclic Dinucleotide Vaccine Adjuvants. *Vaccines (Basel)*. 2020;8(3):453.
94. Taranejoo S, Liu J, Verma P, Hourigan K. A review of the developments of characteristics of PEI derivatives for gene delivery applications. *J Appl Polym Sci*. 2015;132(25):42096.
95. Petrovic M, Borchard G, Jordan O. Considerations for the delivery of STING ligands in cancer immunotherapy. *J Control Release*. 2021;339:235-247.
96. Li W. GALA: a designed synthetic pH-responsive amphipathic peptide with applications in drug and gene delivery. *Adv Drug Deliv Rev*. 2004;56(7):967-985.
97. Nakase I, Kogure K, Harashima H, Futaki S. Application of a Fusiogenic Peptide GALA for

Intracellular Delivery. *Methods Mol Biol*. 2011;683:525-533.

98. Morishita M, Takahashi Y, Nishikawa M, Ariizumi R, Takakura Y. Enhanced Class I Tumor Antigen Presentation via Cytosolic Delivery of Exosomal Cargos by Tumor-Cell-Derived Exosomes Displaying a pH-Sensitive Fusogenic Peptide. *Mol Pharm*. 2017;14(11):4079-4086.
99. Hagino Y, Khalil IA, Kimura S, Kusumoto K, Harashima H. GALA-Modified Lipid Nanoparticles for the Targeted Delivery of Plasmid DNA to the Lungs. *Mol Pharm*. 2021;18(3):878-888.
100. Kawamoto Y, Liu W, Yum JH, et al. Enhanced Immunostimulatory Activity of Covalent DNA Dendrons. *ChemBioChem*. 2022;23(4).
101. Zinchuk V, Zinchuk O, Okada T. Quantitative Colocalization Analysis of Multicolor Confocal Immunofluorescence Microscopy Images: Pushing Pixels to Explore Biological Phenomena. *Acta Histochem Cytochem*. 2007;40(4):101-111.
102. Renault K, Fredy JW, Renard PY, Sabot C. Covalent Modification of Biomolecules through Maleimide-Based Labeling Strategies. *Bioconjug Chem*. 2018;29(8):2497-2513.
103. Hansen RA, Märcher A, Gothelf KV. One-Step Conversion of NHS Esters to Reagents for Site-Directed Labeling of IgG Antibodies. *Bioconjug Chem*. 2022;33(10):1811-1817.
104. Patel H, Tscheka C, Heerklotz H. Characterizing vesicle leakage by fluorescence lifetime measurements. *Soft Matter*. 2009;5(15):2849.
105. Vincent J, Adura C, Gao P, et al. Small molecule inhibition of cGAS reduces interferon expression in primary macrophages from autoimmune mice. *Nat Commun*. 2017;8(1):750.
106. Marcus A, Mao AJ, Lensink-Vasan M, Wang L, Vance RE, Raulet DH. Tumor-Derived cGAMP Triggers a STING-Mediated Interferon Response in Non-tumor Cells to Activate the NK Cell Response. *Immunity*. 2018;49(4):754-763.e4.
107. Corrales L, Glickman LH, McWhirter SM, et al. Direct Activation of STING in the Tumor Microenvironment Leads to Potent and Systemic Tumor Regression and Immunity. *Cell Rep*. 2015;11(7):1018-1030.
108. Jing W, McAllister D, Vonderhaar EP, et al. STING agonist inflames the pancreatic cancer immune microenvironment and reduces tumor burden in mouse models. *J Immunother Cancer*. 2019;7(1):115.
109. Harlin H, Meng Y, Peterson AC, et al. Chemokine Expression in Melanoma Metastases Associated with CD8+ T-Cell Recruitment. *Cancer Res*. 2009;69(7):3077-3085.
110. Henke E, Perk J, Vider J, et al. Peptide-conjugated antisense oligonucleotides for targeted inhibition of a transcriptional regulator in vivo. *Nat Biotechnol*. 2008;26(1):91-100.
111. Ming X, Alam MR, Fisher M, Yan Y, Chen X, Juliano RL. Intracellular delivery of an antisense oligonucleotide via endocytosis of a G protein-coupled receptor. *Nucleic Acids Res*. 2010;38(19):6567-6576.
112. Ämmälä C, Drury WJ, Knerr L, et al. Targeted delivery of antisense oligonucleotides to pancreatic

β-cells. *Sci Adv*. 2018;4(10).